

2015

Simulation of ventilation distribution and gas transport during oscillatory ventilation

<https://hdl.handle.net/2144/13667>

"Downloaded from OpenBU. Boston University's institutional repository."

BOSTON UNIVERSITY
COLLEGE OF ENGINEERING

Thesis

**SIMULATION OF VENTILATION DISTRIBUTION AND
GAS TRANSPORT DURING OSCILLATORY VENTILATION**

by

JACOB HERRMANN

B.S., Boston University, 2012

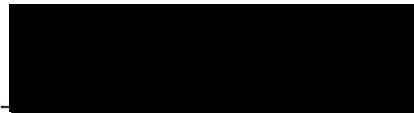
Submitted in partial fulfillment of the
requirements for the degree of
Master of Science

2015

© 2015 by
JACOB HERRMANN
All rights reserved

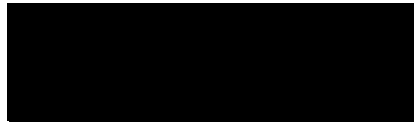
Approved by

First Reader



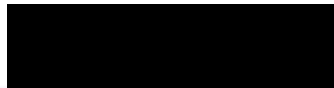
David W. Kaczka, M.D., Ph.D.
Associate Professor – Department of Anesthesia
The University of Iowa Hospital and Clinics

Second Reader



Béla Suki, Ph.D.
Professor of Biomedical Engineering

Third Reader



Joe Tien, Ph.D.
Associate Professor of Biomedical Engineering

Fourth Reader



J. Jane Pillow, BMedSci, MBBS, FRACP, Ph.D.
Associate Professor – School of Anatomy, Physiology, and Human
Biology
The University of Western Australia

Fifth Reader



Brett A. Simon, M.D., Ph.D.
Director – Josie Robertson Surgery Center
Memorial Sloan Kettering Cancer Center

DEDICATION

This thesis work is dedicated to my parents and my grandmother,
whose unconditional love and faith
are a light for me in dark places, when all other lights go out.

Also, shout-outs to:

Alex – thanks

Katie – eating elephants

ACKNOWLEDGMENTS

To my mentor – Dave: for your infinite patience and experienced guidance, for seeing potential in me, and for giving me the opportunity to pursue that potential. I never thought my education would take me in this direction, but I am eternally grateful to you for the purpose and fulfillment I find in our work, and for your unwavering support in this endeavor.

To my committee members – Béla, Joe, Jane, Brett: for your time, for your wisdom, and for your willingness to come together on this project across the divides of time and space.

To my fellow lab members – Reza, Jarred, John, Ashley: for your minds, for your ears, and for the countless hours we toiled away together. Reza and Ashley, your efforts laid the foundation for this work.

To Merryn Tawhai: for your contributions to the development of our model – we are deeply grateful for your collaboration.

To Boston University: for your generosity, and for being my home over the last six years.

**SIMULATION OF VENTILATION DISTRIBUTION AND
GAS TRANSPORT DURING OSCILLATORY VENTILATION**

JACOB HERRMANN

Boston University College of Engineering, 2015

Major Professor: David W. Kaczka, M.D., Ph.D.
Associate Professor – Department of Anesthesia
The University of Iowa Hospital and Clinics

ABSTRACT

High frequency oscillatory ventilation (HFOV) relies on low tidal volumes cycled at supraphysiologic rates, producing fundamentally different mechanisms for gas transport and exchange compared to conventional mechanical ventilation. Despite the appeal of using low tidal volumes to mitigate the risks of ventilator-induced lung injury (VILI), HFOV does not improve mortality in most clinical applications. One possible explanation for this is that HFOV distributes flows throughout the lung in a non-uniform and frequency-dependent manner, especially in the presence of mechanical heterogeneity. This thesis is a systematic investigation of the relationship between carbon dioxide elimination and frequency content during oscillatory ventilation, with emphasis on the frequency-dependent effects of mechanical heterogeneity and various gas transport mechanisms. A computational model consisting of an anatomically-structured airway network was used to simulate ventilation distribution and gas exchange in a canine lung. These simulations were validated against theoretical predictions and experimental data for eucapnic oscillatory ventilation. The model was also

used to assess the impact of mechanical heterogeneity on ventilation distribution and gas transport. Simulations demonstrated a critical transition at the resonant frequency, above which the ventilation patterns became spatially clustered and frequency-dependent. Finally, the model demonstrated that pairs of oscillatory frequencies could yield eucapnic conditions with less potential for VILI compared to traditional single frequency HFOV. These results illustrate the importance of frequency selection in managing the distribution of ventilation and gas transport in the heterogeneous lung, and suggest that the frequency content in oscillatory waveforms may be optimized to achieve eucapnic gas exchange using less injurious ventilation.

TABLE OF CONTENTS

DEDICATION	iv
ACKNOWLEDGMENTS	v
ABSTRACT.....	vi
TABLE OF CONTENTS.....	viii
LIST OF TABLES	x
LIST OF FIGURES	xi
GLOSSARY	xv
1. INTRODUCTION	1
1.1. Background.....	1
1.1.1. The Complications of Mechanical Ventilation.....	1
1.1.2. The Potential of High Frequency Oscillatory Ventilation	4
1.1.3. Gas Transport Mechanisms.....	10
1.2. Objective.....	16
1.3. Rationale	19
2. METHODS	21
2.1. Ventilation Distribution in an Anatomic Model	21
2.1.1. Overview.....	21
2.1.2. Airways.....	21
2.1.3. Acini.....	24
2.1.4. Pleural Pressure.....	26
2.1.5. Injury.....	26
2.1.6. Impedance.....	27
2.1.7. Ventilation distribution	28
2.1.8. Personal Dead Space.....	29
2.2. Gas Transport During Oscillatory Flow	30
2.2.1. Transport Resistance in Branching Network	30
2.2.2. Diffusive/Dispersive Transport Resistance.....	33
2.2.3. Mixing Transport Resistance	37
2.2.4. Total Transport Resistance	42
2.2.5. Direct Alveolar Ventilation.....	42
2.3. List of Simulations.....	44
3. RESULTS	46
3.1. Model Validation	46

3.2.	Impact of Mechanical Heterogeneity	53
3.3.	Comparison of Single and Multiple Frequency Oscillation	57
4.	DISCUSSION	62
4.1.	Model Validation	62
4.2.	Impact of Mechanical Heterogeneity	64
4.3.	Comparison of Single and Multiple Frequency Oscillation	66
4.4.	Limitations	68
5.	CONCLUSION.....	70
5.1.	Summary	70
5.2.	Future Work	71
	APPENDIX.....	73
	Pseudo-code for processing pipeline.....	73
	BIBLIOGRAPHY	74
	CURRICULUM VITAE.....	85

LIST OF TABLES

Table 1. Regression parameters of Equation 54, expected and estimated values for low-frequencies ($f < 1$ Hz).....	51
Table 2. Simulation parameters and statistics for comparison of single- and multi-frequency ventilation. Shading indicates data represented by same colors in Figure 22.	60

LIST OF FIGURES

Figure 1. ARDS classification by the Berlin Definition based on observed PaO ₂ :FiO ₂ ratio (71).....	1
Figure 2. Idealized representation of VILI risk reduction during HFOV compared to CMV. High mean airway pressure maintains recruitment and low tidal volume avoids overdistension.	5
Figure 3. Mechanisms of gas transport in the airways and acinar spaces during high frequency oscillatory ventilation, depicted at relative locations of greatest influence. Reproduced from Slutsky and Drazen (81).....	11
Figure 4. Proposed mechanism of benefit for multiple frequency oscillatory ventilation of mechanically heterogeneous lungs: lung regions with different mechanical properties selectively filter input multi-frequency oscillations, such that the resulting ventilation distribution is uniform in all regions.	18
Figure 5. Segmented central airways from 3DCT scan of 25 kg dog at 30 cmH ₂ O distending pressure (left) and generated network of cylinders used in computational model (right).	22
Figure 6. Circuit representation of an airway segment element. Input flow at the proximal node is divided between parallel shunt pathways of gas compression and wall distension, and the subtending airway subtrees at the distal node. Equations Equation 13 and Equation 14 provide the impedance for Zlong and Zshu, respectively.	24
Figure 7. Circuit representation of an acinar element. Input flow at the proximal node is divided between parallel pathways of gas compression compliance and acinar volume expansion, whose impedance is modeled by a constant phase element described in equations Equation 16 and Equation 17.....	25
Figure 8. Heterogeneous lung injury is simulated by scaling tissue elastance according to gravitationally-weighted gradient noise, which produces a cloudy, heterogeneous texture. The color of each acinar element corresponds to the ratio of tissue elastance H _{injured} /H _{healthy} . The direction of gravitational force (g) is indicated by the arrow.....	27
Figure 9. Simplified representation of transport resistances in a model bifurcation and the corresponding system of linear equations representing the mesh analysis approach to solving for molar fluxes.....	32
Figure 10. Model of an airway segment with reservoirs at either end containing the same gas species at different concentrations (color used only to clarify	

different concentrations – color does not indicate different species). A volume of gas is oscillated through the segment, and the volume of gas that passes completely through the segment is available for mixing with the opposing reservoir.....	38
Figure 11. Illustration of method for computing V_{mix} during ventilation with multiple frequencies of oscillation. In this example, two frequencies are used, 3Hz and 7Hz, and $f_0 = 1$ Hz. The light red shading indicates where the conditions of $V_t > 0$ (top) and $V(t) > V_{seg}$ (bottom) are satisfied. V_{mix} can be calculated in two ways: from the flow integral indicated by dark red shading (where both conditions are satisfied), or from the length of the red lines (i.e. local maxima of $V_t - V_{seg}$).	41
Figure 12. Modeling the distribution of airway segment volumes (i.e. personal dead space, VD^*) and inspired fresh gas volume (V_f) to each individual acinar compartment. Acini are modeled with tissue elastance and end-expiratory residual volume. Although fresh gas is assumed to have zero pCO_2 , at end-inspiration the gas contents are assumed to be well-mixed. Note that the distribution of inspired volumes is predicted to be non-uniform in the presence of heterogeneous mechanics. Figure reproduced from Colletti <i>et al.</i> (18).	43
Figure 13. Relationship between VCO_2 and VT for a variety of frequencies, each value of f indicated by color. The black lines represent the lower bound of VCO_2 produced by molecular diffusion alone (zero-flow conditions), and the prediction of required VCO_2 for eucapnic equilibrium.	47
Figure 14. Isolated data of simulations for 0.1 Hz oscillations, with text labels indicating the volume amplitude ranges over which certain gas transport mechanisms dominate overall VCO_2 .	48
Figure 15. Interpolated contours of VCO_2 over the $VT - f$ plane, bi-linearly interpolating between the discrete pairs of VT and f chosen for simulations (indicated by white circles). The black line indicates the prediction of required VCO_2 for eucapnia.	49
Figure 16. Power-law regressions to eucapnic tidal volume requirements over localized frequency ranges. The black line represents the interpolated contour of eucapnic ventilation parameters. The red line is regressed over $0.1 \text{ Hz} < f < 1 \text{ Hz}$, and the blue line over $2 \text{ Hz} < f < 30 \text{ Hz}$. These frequency ranges are indicated by light shading.	49
Figure 17. Comparison between the simulation data from this model and the experimental data collected and regressed by Venegas <i>et al.</i> (97). The axes are dimensionless variables of frequency (F) and flow (Q). The black lines	

correspond to theoretical prediction of low-frequency gas exchange (dashed) and regression to experimental HFOV data (solid). The red line represents the simulation results interpolated at eucapnic conditions. 52

Figure 18. Acinar distribution histograms at each simulated frequency for healthy conditions. Flow magnitude (top) is normalized to a uniform distribution (i.e. unity corresponds to acinar magnitude equal to tracheal magnitude divided by the total number of acini). Flow phase (middle) is normalized to the phase of the input flow at the trachea (i.e. zero corresponds to acinar flow in phase with tracheal flow). CO₂ elimination (bottom) is normalized to a uniform distribution (i.e. unity corresponds to acinar VCO₂ equal to VCO₂euc divided by the total number of acini). Vertical black line indicates resonant frequency (f_{res} : elastic and inertial components of impedance equal and opposite). 54

Figure 19. Acinar distribution histograms at each simulated frequency for injured conditions. Flow magnitude (top) is normalized to a uniform distribution (i.e. unity corresponds to acinar magnitude equal to tracheal magnitude divided by the total number of acini). Flow phase (middle) is normalized to the phase of the input flow at the trachea (i.e. zero corresponds to acinar flow in phase with tracheal flow). CO₂ elimination (bottom) is normalized to a uniform distribution (i.e. unity corresponds to acinar VCO₂ equal to VCO₂euc divided by the total number of acini). Vertical black line indicates resonant frequency (f_{res} : elastic and inertial components of impedance equal and opposite). 55

Figure 20. (A) Frequencies of maximum and minimum normalized flow magnitude, shown for clarity in the context of a single acinus. (B) Frequencies of maximum (top) and minimum (bottom) normalized flow magnitude, represented spatially for every acinus, using consistent coloring according to the scale provided in (A). Acini which do not exhibit a local minimum or maximum within the range of frequencies simulated are shown in black. Results shown for healthy (left) and injured (right) conditions. 56

Figure 21. Ventilation distribution similarity, assessed per the contours of VDIP for each permutation of two frequencies, for healthy (left) and injured (right) conditions at mean airway pressure. Note: the values are symmetric about the line of identity $f_1 = f_2$. Frequency pairs chosen for multiple frequency oscillatory ventilation gas transport simulations indicated by crossed circles. 57

Figure 22. Histograms of acinar CO₂ elimination (top) and root-mean-square volume (bottom), normalized to the uniform distribution (i.e. unity corresponds to tracheal value divided by the total number of acini). Lightly colored lines represent raw histogram data with 1000 logarithmically spaced

bins between 0.1 and 10; dark lines represent smoothed histogram data, shown for clarity. Blue: single frequency 11 Hz; red: single frequency 24 Hz; fuchsia: multi-frequency 11 Hz and 24 Hz. Histograms calculated from simulations resulting in eucapnic ventilation conditions (within 5% tolerance of V_{CO2euc}). Required eucapnic tidal volume V_T for each condition and statistical results provided in Table 2..... 59

Figure 23. Quantiles of root-mean-square volume, normalized to the uniform distribution (i.e. unity corresponds to tracheal value divided by the total number of acini). Blue: single frequency 11 Hz; red: single frequency 24 Hz; fuchsia: multi-frequency 11 Hz and 24 Hz. The colored data points correspond to the histograms represented in Figure 22 and shaded cells of Table 2. The shaded gray region represents 90% of all acini. Quantiles calculated from simulations resulting in eucapnic ventilation conditions (within 5% tolerance of V_{CO2euc} . Required eucapnic tidal volume V_T for each condition and statistical results provided in Table 2. 61

GLOSSARY

ARDS	acute respiratory distress syndrome	D_{eff}	effective diffusivity
\dot{V}/\dot{Q}	ventilation-perfusion ratio	f_c	corner frequency
$\text{PaO}_2:\text{FiO}_2$	ratio of PaO_2 to FiO_2	\dot{M}	mass flux
PaO_2	arterial partial pressure of oxygen	A_{CS}	cross-sectional area
FiO_2	inspired oxygen fraction	L	length
VILI	ventilator-induced lung injury	\bar{c}	mean-axial concentration
VALI	ventilator-associated lung injury	D	diffusion coefficient
CMV	conventional mechanical ventilation	D_{mol}	molecular diffusivity
PEEP	positive end-expiratory pressure	D_{dis}	dispersion coefficient
CT	computed tomography	\bar{U}	mean-axial velocity
V_T	tidal volume	r	radius
SIMV	synchronized intermittent mandatory ventilation	Re	Reynolds number
PaCO_2	arterial partial pressure of carbon dioxide	α_W	Womersley number
HFOV	high frequency oscillatory ventilation	Sc	Schmidt number
O_2	oxygen	ρ	density
CO_2	carbon dioxide	μ	dynamic viscosity

V_D	dead space volume	ν	kinematic viscosity
f	frequency	ω	angular frequency
\dot{V}_{CO_2}	rate of CO ₂ elimination	MFOV	multi-frequency oscillatory ventilation
HFPV	high frequency percussive ventilation	P_{acn}	acinar pressure
SFOV	single frequency oscillatory ventilation	P_{pl}	pleural pressure
3DCT	three-dimensional computed tomography	Z_{sub}	subtree (inclusive) impedance
Z_{long}	airway longitudinal impedance	$Z_{sub,child(n)}$	Z_{sub} for n^{th} child of parent segment
Z_{shu}	airway shunt impedance	∇c	concentration gradient
F_c	airway wall cartilage fraction	p	partial pressure
R_s, R_c	soft & cartilaginous wall resistance	R_T	transport resistance
I_s, I_c	soft & cartilaginous wall inertance	R_{gas}	universal gas constant
C_s, C_c	soft & cartilaginous wall compliance	T	absolute temperature
C_g	gas compression compliance	\mathbf{R}_T	transport resistance matrix
V_{seg}	airway segment volume	\mathbf{M}	mass flux vector
P_{seg}	airway segment distending pressure	Δp	partial pressure difference vector
Z_{acn}	acinus impedance	R_T^{diff}	diffusive transport resistance
G	tissue damping	u	velocity

H tissue elastance	c concentration of gas
η tissue hysteresivity	t time
α oscillation frequency exponent	R_T^{tot} total transport resistance
P pressure	f_{res} resonant frequency
P_{tp} transpulmonary pressure	f_{min} frequency of local minimum flow magnitude
X example gas	f_{max} frequency of local maximum flow magnitude
n number of moles of gas	VDIP ventilation distribution inner product
V volume of gas	V_D^* personal dead space volume
V_{osc} oscillatory volume	
f_0 fundamental frequency	
F molar fraction of gas	
R_T^{mix} mixing transport resistance	
V_{mix} oscillatory volume available for mixing	
V_{peak} peak oscillatory mixing volume	

1. INTRODUCTION

1.1. BACKGROUND

1.1.1. *The Complications of Mechanical Ventilation*

Acute respiratory distress syndrome (ARDS) is a devastating condition with a mortality rate near 40 percent, and an estimated incidence of 200,000 cases per year in the United States (100). ARDS is associated with widespread, localized atelectasis and alveolar edema, inducing substantial mechanical heterogeneity in the parenchyma, resulting in ventilation-perfusion (\dot{V}/\dot{Q}) mismatching in the lung (53, 54). ARDS is clinically assessed by the ratio of arterial oxygen tension to the fraction of inspired oxygen (PaO₂:FiO₂ ratio). In the Berlin Definition, the ARDS Definition Task Force classifies ARDS as mild, moderate, or severe depending on the PaO₂:FiO₂ ratio below 300 mmHg, as summarized in Figure 1 (71, 99).

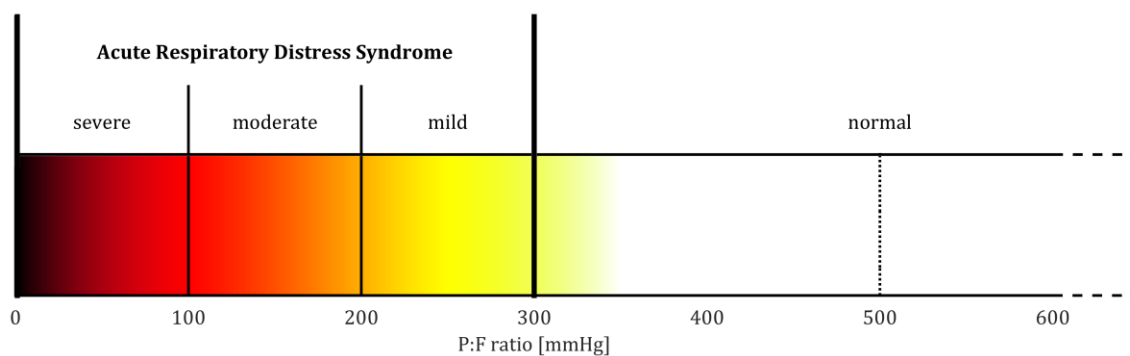


Figure 1. ARDS classification by the Berlin Definition based on observed PaO₂:FiO₂ ratio (71).

Mechanical ventilation is a necessary, life-sustaining intervention for patients who lose the ability to maintain adequate gas exchange. However, mechanical

ventilation may also worsen existing injury and/or induce additional injury *via* ventilator-induced lung injury (VILI). Conventional mechanical ventilation (CMV) uses tidal volumes and respiratory rates similar to those of normal spontaneous breathing, accompanied by positive end-expiratory pressure (PEEP) to maintain lung recruitment and increased FiO_2 to maintain oxygenation. Lung-protective ventilation relies on smaller tidal volumes and higher PEEP to minimize the risk of VILI occurring (93). Optimal ventilator settings are difficult to determine for a specific patient without invasive measurements (i.e. esophageal balloon catheter, X-ray CT imaging, etc.) (12, 89). Such settings may require further adjustments over time as the patient's condition fluctuates. For example, insufficient tidal volume (V_T) results in hypercarbia, yet excessive V_T leads to VILI *via* overdistension (volutrauma). Insufficient PEEP leads to collapse or edema of atelectatic tissue and/or cyclical recruitment and collapse (atelectrauma), yet excessive PEEP causes increased lung elastance and increases the risk of overdistension.

Volutrauma and atelectrauma may occur simultaneously in mechanically ventilated patients due to increased mechanical heterogeneity of parenchymal tissues (12). Increased transpulmonary pressure gradients lead to substantial derecruitment of dependent regions and overdistension of non-dependent regions. Tidal volumes that cannot be distributed to non-recruitable tissues instead overdistend tissues already recruited by PEEP (33, 62, 66).

Ventilator-associated lung injury (VALI) is a more appropriate term than VILI

in some settings because it is difficult to attribute worsening lung injury to mechanical ventilation as opposed to the underlying condition. VALI occurs most commonly in patients suffering from ARDS due to both mechanical heterogeneity in the lungs and disease severity, and VALI results in a progressively worsening condition (32, 83, 106). Although maintaining gas exchange is the primary goal of mechanical ventilation, it is imperative that the risk of VILI be minimized through appropriate management of ventilator settings as well as through the use of optimal ventilation strategies. Thus, optimizing lung-protective mechanical ventilation requires careful consideration of not only the effects of individual ventilator settings, but also the interactions between the effects. Additionally, extreme mechanical heterogeneity limits the extent to which the risk of VILI can be mitigated by lung-protective ventilation.

Until recently, mortality in ARDS patients was near 40 percent, with the leading cause of death being multiple organ failure and sepsis. Respiratory failure was deemed the primary cause of death for under one fifth of the mortalities (7, 9, 26, 63, 86). While advances in treatment and ventilation strategies have reduced overall mortality to near 30 percent, the causes of death have remained relatively unchanged, with multiple organ failure and sepsis as the leading cause and respiratory failure comparatively low (24, 86, 105). In 1990 and 1994, Hickling demonstrated reduced mortality using a “permissive hypercapnia” strategy, in which reduced tidal volumes given *via* synchronized intermittent mandatory ventilation (SIMV) result in improved mortality despite

elevated PaCO₂ (44, 45). However, the seminal ARDS Network study in 2000 demonstrated similar reductions in mortality without hypercapnia, using a PEEP-FiO₂ ladder as well as reduced tidal volumes and increased respiratory rates – a protocol that has become the clinical standard in ARDS treatment (93). These studies of low tidal volume ventilation demonstrate that ventilation strategies specifically designed to minimize VILI reduce mortality. Furthermore, multiple organ failure and sepsis, the leading causes of death for ARDS, are directly associated with injurious ventilation due to the release of inflammatory mediators (biotrauma) (70). It follows that the greatest improvement in outcomes results from ventilator strategies that minimize VILI while maintaining adequate gas exchange.

1.1.2. The Potential of High Frequency Oscillatory Ventilation

High frequency oscillatory ventilation (HFOV) has been of interest for treatment of ARDS since it was first introduced in animal studies in the 1980's (8, 75, 80). As shown in Figure 2, the ability to maintain oxygenation and CO₂ elimination using tidal volumes smaller than anatomic dead space reduces the potential for VILI, thereby improving outcomes for ARDS patients.

Prior to experimental evidence for the feasibility of HFOV, direct alveolar ventilation *via* bulk advection was considered the only viable mechanism of gas transport between the alveolar spaces and the airway opening. This is essentially true for large tidal volumes delivered at low respiratory rates (f) (i.e., during normal breathing and CMV with $f < 0.67$ Hz or 40 min⁻¹). HFOV instead relies

on alternate convective mechanisms to maintain oxygenation and CO₂ elimination. During large- V_T low- f ventilation, the rate of CO₂ elimination (\dot{V}_{CO_2}) is proportional to direct alveolar ventilation, which is defined as the volume of fresh gas delivered past the dead space volume (V_D), estimated by the following relationship:

$$\dot{V}_{CO_2} \propto f(V_T - V_D) \quad \text{Equation 1}$$

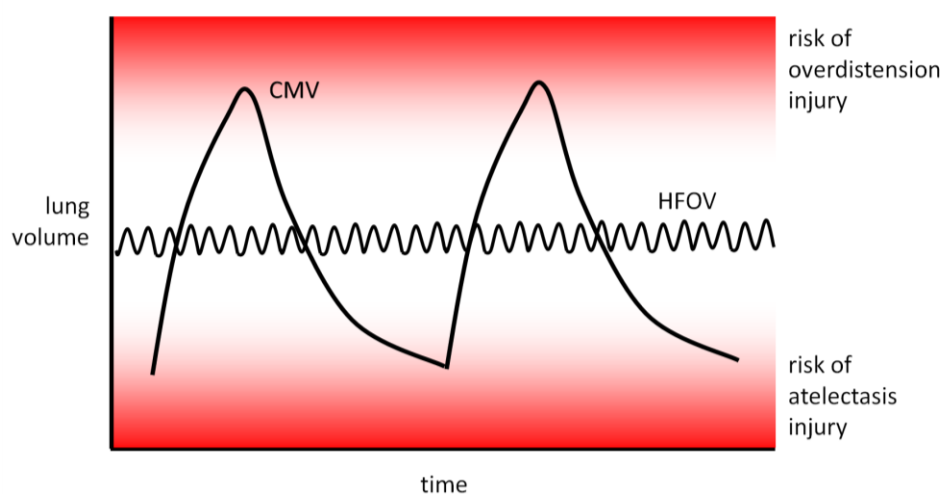


Figure 2. Idealized representation of VILI risk reduction during HFOV compared to CMV. High mean airway pressure maintains recruitment and low tidal volume avoids overdistension.

Maintenance of oxygenation and CO₂ elimination are the ultimate gas exchange priorities of mechanical ventilation. Gas transport during conventional ventilation (i.e. large- V_T low- f) occurs primarily *via* advection, or the transport of mass due to bulk motion. Gas transport must occur across the dead space volume, which under normal circumstances comprises the volume of conducting airways, and does not participate in gas exchange with pulmonary capillaries. Extremes of O₂ concentration gradients imposed with high FiO₂ increase

diffusion and uptake of O_2 . However, there is no such method available to increase the reverse CO_2 gradient because atmospheric concentrations of CO_2 are already minimal (approximately 0.04 % or 0.3 mmHg partial pressure at sea level). Therefore, adequate CO_2 transport across the dead space can only be maintained through the appropriate selection of V_T and f .

The optimal combination of V_T and f is both patient-specific and case-specific, determined by the anatomy of the conducting airways as well as the impact of injury on the mechanical properties of the lung tissues and airways. Lung-protective ventilation, using high PEEP and low V_T , requires higher-than-normal respiratory rates to maintain adequate CO_2 elimination. Despite using higher rates than conventional ventilation, gas transport during lung-protective ventilation is still appropriately assumed advection-dominated, and therefore implemented according to the relationship in Equation 1.

Diffusion in the mammalian airway tree was initially presumed a minor component of gas transport compared to advection, since the molecular diffusivity of CO_2 in air is insufficient to maintain normocarbina. However, *in vivo* experiments using tidal volumes less than anatomic dead space and high frequencies (i.e. $f > 1\text{Hz}$) demonstrated that convection, which involves both advection and diffusion, can be a viable means of gas transport when neither advection nor diffusion alone are sufficient (8, 75). Clearly, those results do not coincide with Equation 1, and so it must be that diffusion is enhanced during HFOV, such that both advective and diffusive transport contribute significantly to

the movement of CO₂. Theoretical (29, 34, 49, 67) and experimental (82, 97) studies established a relationship between ventilatory parameters and CO₂ elimination, which in contrast to Equation 1 is quantified an efficiency term that relates the effective diffusivity (D_{eff}) of CO₂ in the lung to V_T and f :

$$D_{\text{eff}} \propto f^a V_T^b \quad \text{Equation 2}$$

The values of a and b in Equation 2 depend on a variety of factors (e.g. flow velocity profile, Taylor dispersion, asynchronous gas mixing, etc.), though it has been consistently demonstrated that $a < b$ (13, 68). In their study, Venegas *et al.* collected data from a variety of mammalian species, and computed dimensionless frequency (\mathcal{F}) and flow (\mathcal{Q}) parameters during eucapnic ventilation (97):

$$\mathcal{F} = f \frac{V_D}{\dot{V}_A} \quad \text{Equation 3}$$

$$\mathcal{Q} = f \frac{V_T}{\dot{V}_A} \quad \text{Equation 4}$$

where \dot{V}_A is eucapnic alveolar ventilation described by:

$$\dot{V}_A = 863 \frac{\dot{V}_{\text{CO}_2}^{\text{euc}}}{\text{PaCO}_2} \quad \text{Equation 5}$$

Venegas *et al.* proposed two dimensionless equations for gas transport: at low frequencies $\mathcal{Q} = 1 + \mathcal{F}$ corresponds directly to Equation 1, and at high frequencies $\mathcal{Q} = c_0 \mathcal{F}^{c_1}$ is a regression to the experimental data (justified by qualitative inspection), with $c_0 = 0.40$ and $c_1 = 0.54$. Due to the greater dependence of CO₂ elimination on V_T rather than f during HFOV, and due to the frequency-dependent pressure cost of ventilation (i.e. the amplitude of distending pressures

experienced by mechanically-vulnerable lung tissues), clinical strategies preferentially adjust V_T while maintaining f near the corner frequency (f_c), below which the pressure cost of ventilation is most sensitive to changes in frequency (68, 96).

Animal studies of HFOV demonstrate improvements in oxygenation and reductions in lung inflammation (51, 64). However the successful outcomes found using HFOV in animal models of ARDS did not translate to improved mortality in clinical studies. HFOV treatment in infant (35, 69, 94), pediatric (4, 39, 74), and adult (10, 20, 25, 104) ARDS results in improved oxygenation yet highly variable outcomes with respect to mortality. Recent meta-analyses for infant (19), pediatric (87), and adult (38, 46, 87) clinical trials of HFOV use in ARDS treatment conclude no significant difference in mortality. As a result HFOV is presently considered a rescue therapy for refractory hypoxemia used only when CMV or lung-protective ventilation fail, most notably in neonatal care. However HFOV use in ARDS patients is still subject to much controversy. There is currently no universally-accepted “best practice” for HFOV treatment involving selection of ventilator settings, medication provided, time to intervention after diagnosis, duration of HFOV, and patient selection. Further studies may elucidate the impact of differences in protocol: for example, the OSCILLATE trial in adults demonstrated increased mortality in the HFOV treatment group, which may be attributed to excessive distending pressure and consequent need for increased use of pressors, sedatives, or neuromuscular blockade (25). Another

instructive example is the HIFI trial in infants: a low lung volume strategy (i.e. low distending pressure) and conservative use of recruitment maneuvers during HFOV resulted in detrimental outcomes, which may be attributed to a lack of sustained recruitment (94). Reviews of clinical studies suggest that improved outcomes with HFOV may yet be found in appropriate patient selection, better understanding of ARDS etiology and phenotype, and the use of bedside technology to monitor lung volumes (i.e. electrical impedance tomography, plethysmography) (9, 61, 98).

HFOV strategies allocate little consideration to the impact of mechanical heterogeneity on the frequency-dependence of the ventilation distribution (1, 17). Most clinical trials report arbitrary initial values for frequency, with subsequent adjustments based on patient needs and Equation 2 (21). The lack of a mechanistically-based protocol may be due in part to the lack of clinical technology for assessing frequency-dependent mechanics at the bedside, or the difficulty of making such measurements in critically ill patients. The initial selection of frequency is usually in the vicinity of f_c for an average adult human with ARDS, which falls within an ideal range according to the strategy of minimizing the pressure cost of ventilation (68, 96). However, the specific choice of frequency can substantially alter the distribution of flow throughout the airways, especially in the presence of heterogeneous lung injury (1, 17). Equation 1 and Equation 2 may be specific cases of a more generalized relationship between gas transport and ventilatory parameters, and thus may not apply

directly to mechanically heterogeneous lungs. In developing optimal HFOV strategies, it is necessary to consider the physical mechanisms of gas transport, and how they are affected by such heterogeneity.

1.1.3. Gas Transport Mechanisms

The mechanisms of gas transport through the conducting airways during oscillatory flow is attributed to several dominating convective processes (13, 68):

- 1) direct alveolar ventilation *via* advection
- 2) asymmetric velocity profiles, inspiratory-expiratory differences in velocity profiles
- 3) turbulent and oscillatory dispersion
- 4) out-of-phase oscillation, Pendelluft phenomenon
- 5) cardiogenic mixing
- 6) collateral ventilation
- 7) molecular diffusion

The magnitude of the effect each mechanism has on local gas transport varies depending on surrounding airway geometry, as demonstrated in Figure 3. Direct alveolar ventilation affects the alveoli with the shortest path lengths to the airway opening with the lowest impedance to the input flow, and only for tidal volumes exceeding some patient-specific minimum, which may be proportional to V_D (11, 13, 49). It can be increased by increasing either V_T or f once V_T is sufficiently large, in accordance with Equation 1. Direct alveolar ventilation *via* advection is the fastest possible method of gas transport, although large tidal volumes can be

injurious as previously mentioned. Therefore it is preferable to minimize VILI by finding an alternative to direct alveolar ventilation as the primary means of gas transport.

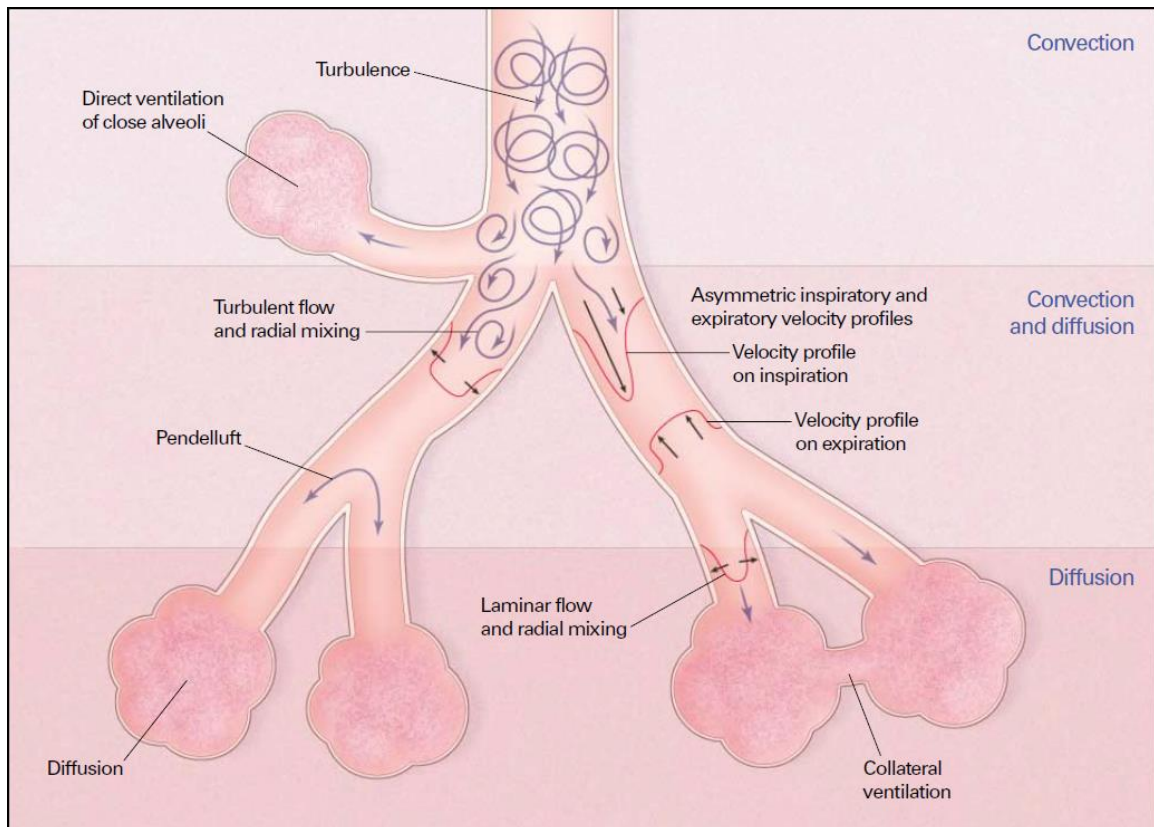


Figure 3. Mechanisms of gas transport in the airways and acinar spaces during high frequency oscillatory ventilation, depicted at relative locations of greatest influence. Reproduced from Slutsky and Drazen (81).

Diffusion governs the rate of mass transport along a concentration gradient.

The molar flux \dot{M} of a species through a tube of length L and cross-sectional area A_{cs} is given by Fick's law of diffusion:

$$\dot{M} = -DA_{cs} \frac{\Delta \bar{c}}{L} \quad \text{Equation 6}$$

where D is the diffusivity and $\Delta \bar{c}$ is the difference in the mean axial concentration across the length of the tube. Molecular diffusion has the most dominant effect

on gas exchange in peripheral airways and alveoli, due to minimal flow rates and large surface area to volume ratio at this level of the airway tree. Molecular diffusivity depends on gas species and temperature, and is usually assumed constant. It cannot be influenced by ventilator settings, although the rate of O₂ transport *via* diffusion can be enhanced *via* increased FiO₂. By contrast, turbulent or oscillatory dispersion, which manifests in steady state as an effective diffusivity, is dependent on local velocity profiles and flow characteristics. Both V_T and f affect the contribution of dispersion to the overall effective diffusivity.

Dispersion was first described by Taylor, characterizing effective steady state longitudinal diffusivity during laminar and turbulent flow (91, 92). In 1956, Aris related the effective diffusivity (D_{eff}) to the sum of a molecular diffusivity (D_{mol}) and a dispersion coefficient (D_{dis}) (2). Chatwin in 1975 provided a derivation for the case of oscillatory dispersion in tubes (14), and Watson later provided a generalized full form of the relative increase factor relating the oscillatory dispersion coefficient to molecular diffusivity (101). A brief summary of these works on dispersion in tubes is summarized in the following set of equations for D_{dis} in terms of fluid mean velocity \bar{U} and tube radius r :

laminar dispersion	$D_{\text{dis}} = \frac{(\bar{U}r)^2}{D_{\text{mol}}} \cdot \frac{1}{48}$	Equation 7
-----------------------	---	------------

turbulent dispersion	$D_{\text{dis}} = \bar{U}r \cdot \beta_1(\text{Re})$	Equation 8
-------------------------	--	------------

oscillatory dispersion	$D_{\text{dis}} = \frac{(\bar{U}_{\text{rms}}r)^2}{D_{\text{mol}}} \cdot \beta_2(\alpha_W, \text{Sc})$	Equation 9
---------------------------	--	------------

where Re is the Reynolds number, characterizing the ratio of inertial force to viscous force in steady flows (73):

$$\begin{array}{l} \text{Reynolds} \\ \text{number} \end{array} \quad Re = \frac{2 \rho \bar{U} r}{\mu} = \frac{2 \bar{U} r}{\nu} \quad \text{Equation 10}$$

and α_W is the Womersley number, characterizing the ratio of inertial force to viscous force in oscillatory flows (103):

$$\begin{array}{l} \text{Womersley} \\ \text{number} \end{array} \quad \alpha_W = r \sqrt{\frac{\rho \omega}{\mu}} = r \sqrt{\frac{\omega}{\nu}} \quad \text{Equation 11}$$

Sc is the Schmidt number, which characterizes the ratio of viscous diffusion rate to molecular diffusion rate (48):

$$\begin{array}{l} \text{Schmidt} \\ \text{number} \end{array} \quad Sc = \frac{\mu}{\rho D_{\text{mol}}} = \frac{\nu}{D_{\text{mol}}} \quad \text{Equation 12}$$

Re , α_W , and Sc are dimensionless parameters, and relate to scaled geometries and flows with dynamic similarity. ρ is density, μ is dynamic viscosity, ν is kinematic viscosity, and ω is the angular frequency of oscillation. β_1 and β_2 are functions of Re , α_W , and Sc (2, 14, 92, 101).

The Womersley number characterizes the velocity profile and boundary layer thickness during oscillatory flow, with dynamic similarity. At one extreme, $\alpha_W < 1$ represents viscous forces dominating, and produces a parabolic flow profile in phase with pressure oscillations. At the other extreme, $\alpha_W > 10$ represents inertial forces dominating, and produces a plug flow profile which lags pressure oscillations by $\frac{\pi}{2}$ radians. Laminar flow with a flat velocity profile does not contribute to diffusion *via* dispersion. Thus, for $\alpha_W > 10$, D_{dis} approaches zero

and D_{eff} approaches D_{mol} .

Asymmetric velocity profiles resulting from flow division at airway bifurcations increase the effective diffusivity due to the non-flat velocity profile (13, 77), with convective eddies and secondary flows also contributing to enhanced mixing (15, 50, 59). For large tidal volumes, the asymmetry of the velocity profiles is strongest during inspiration, when the airway bifurcations cause flow division. However, expiratory flow profiles are much flatter and more symmetric when flows combine at the bifurcations rather than divide around them (15, 30, 50, 77). The effects of these mechanisms depend on the complicated, three-dimensional geometry of the branching airway network. Accordingly, computational models designed to study these mechanisms employ fluid dynamics solvers. However such solvers incur extreme computational costs, such that the use of supercomputing clusters is required, with the scope of simulations typically restricted to the central airways.

Lung regions with different mechanical time constants can experience out-of-phase flow oscillations, referred to as pendelluft (37, 57, 65, 81). Pendelluft improves the homogeneity of gas concentrations throughout the lung *via* interregional mixing. Collateral ventilation has a similar effect, albeit on a much smaller scale, resulting in inter-alveolar mixing (3). Cardiogenic oscillations, caused by ventricular contractions and relaxations, induce flow and pressure oscillations in lung regions adjacent to the mediastinum (31, 84). Although the magnitude of cardiogenic oscillation is small compared to tidal breathing and

CMV, during HFOV it may contribute significantly to gas transport and interregional mixing (79).

The interactions between the transport mechanisms described here synergistically influence homogenization of gas concentrations throughout the airways. Moreover, the geometric nature of flow-reliant mechanisms localizes their respective contributions to gas transport within differently-sized airways. For example, diffusion dominates transport in the most peripheral airways, which experience small flow amplitudes but have large cumulative cross-sectional area.

Finally, consideration of the physical principles underlying these mechanisms highlights a complicated relationship between gas exchange and ventilator settings. For example, increasing frequency can have both beneficial and detrimental effects on gas transport in different localized geometries: (1) increased rate of direct alveolar ventilation, *à la* Equation 1; (2) increased rate of mixing at airway bifurcations; (3) changes in dispersion coefficients (which can lead to either increased or decreased gas transport, depending on Womersley numbers and velocity profiles for individual airways); and finally (4) changes in regional oscillatory magnitudes and phases due to heterogeneous mechanics and asymmetric branching structures, which also affects the aforementioned responses.

1.2. OBJECTIVE

It is evident that HFOV can provide life-sustaining ventilation using minimal volume oscillations, and therefore has the potential to be clinically useful by minimizing VILI risks during ARDS treatment. However, the development of ventilation strategies requires a comprehensive understanding of V_T - and f -dependent gas transport mechanisms, especially in the injury-relevant context of mechanically heterogeneous lung tissues and airways. Considering the clinical goal of minimizing the risk of VILI *via* overdistension, ventilatory efficiency can be defined in terms of the ability to achieve adequate gas exchange using the smallest possible volume and pressure amplitudes experienced by the vulnerable airways and parenchyma. Taking into account the mechanisms that produce enhanced diffusion and mixing during high frequency oscillations, we propose that optimal ventilation occurs when all alveolar spaces experience the same average volume distension over a period of oscillation. \dot{V}/\dot{Q} mismatching is abundant when the ventilation distribution is heterogeneous, with over-ventilation and under-ventilation occurring simultaneously in different lung regions (6, 36, 102). It follows that uniform ventilation optimizes gas exchange as well as ventilatory efficiency. Therefore, **we hypothesize that optimal gas transport and exchange during oscillatory ventilation occurs when oscillatory flow is distributed most uniformly throughout all conducting airways.** Furthermore, we propose that ventilating a mechanically heterogeneous lung with multiple frequencies of oscillation simultaneously can,

in some cases, produce a more uniform ventilation distribution compared to any single frequency. The mechanical properties of the injured lung are heterogeneous and frequency-dependent (54). Thus, broadband flow and pressure oscillations are selectively and mechanically filtered by distributed regional impedances, such that the ventilation is also distributed in a heterogeneous and frequency-dependent manner (1).

Theoretically, ventilation with multiple frequencies of oscillation can improve the homogeneity of ventilation distribution in mechanically heterogeneous airways and parenchyma, as illustrated in Figure 4. The concept of using simultaneous multiple frequencies of oscillation is directed at optimizing the distribution of flow throughout the airway tree, thereby providing sufficient CO₂ elimination with less potential for injurious ventilation. The strategy of optimizing linear combinations of two or more oscillatory frequencies relies on heterogeneity and frequency-dependence, such that the ventilation distributions at each respective frequency are not similar to each other. Ideal candidate frequencies include those that complement each other: if one frequency causes relative over-ventilation of a particular lung region, the other frequency causes relative under-ventilation in that same region. A linear combination of the two distributions may result in a more homogeneous ventilation overall.

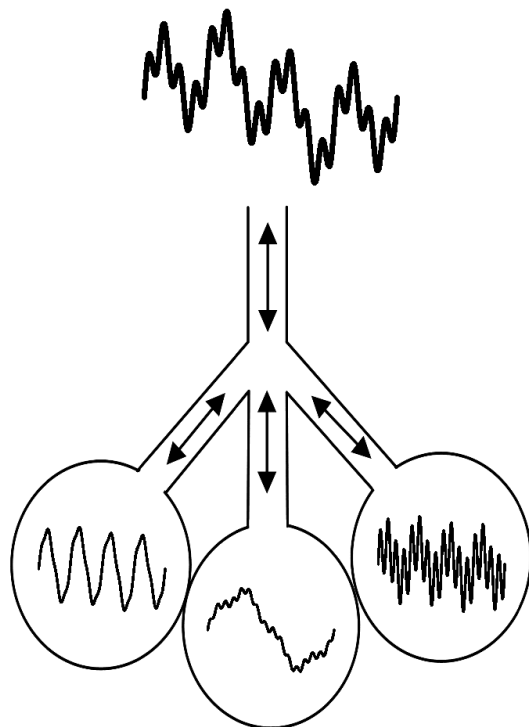


Figure 4. Proposed mechanism of benefit for multiple frequency oscillatory ventilation of mechanically heterogeneous lungs: lung regions with different mechanical properties selectively filter input multi-frequency oscillations, such that the resulting ventilation distribution is uniform in all regions.

To establish support for this hypothesis, we identify three aims:

Aim 1: Develop an anatomic model for ventilation and gas transport valid over a wide range of V_T and f . The construction of this model enables simulations of gas transport during oscillatory ventilation. This model will be used to produce a basis for the hypothesis, founded on established physical principles of gas transport. Model validity will be assessed by comparison of simulation-derived and experiment-derived relationships between f , V_T , V_D , and \dot{V}_{CO_2} during HFOV (97).

Aim 2: Determine the relationship between mechanical heterogeneity and gas transport during traditional HFOV. It is central

to the argument of the hypothesis that traditional HFOV, using a single frequency of oscillation, is an inefficient means of ventilating heterogeneously injured lungs. Therefore, this aim requires simulation of the effects of ARDS on the distribution of mechanical properties of the lung tissues. Ventilatory efficiency will be assessed during HFOV under both healthy and heterogeneously injured conditions.

Aim 3: Compare ventilatory efficiency during ventilation with either one or two frequencies of oscillation. Oscillatory ventilation with multiple frequencies simultaneously is a novel concept, and thus has no precedent in existing literature. This aim requires the model to encompass both (1) established relationships of gas exchange during oscillatory flow, as well as (2) their generalized formulations during multi-frequency oscillatory flow.

Altogether, these aims will evaluate a correlation between ventilation homogeneity and gas transport within a physiologically and anatomically relevant model, and further demonstrate the potential of ventilation with optimized frequency content for the treatment of heterogeneous lung injury.

1.3. RATIONALE

Clinical implementation of HFOV in the treatment of adult patients with heterogeneous lung injury has been tentative, and with good reason. The current expanse of relevant literature neither demonstrates improved outcomes in clinical trials nor offers a systematic study of the frequency-dependent heterogeneity of ventilation distribution and gas transport. The purpose of this

thesis is to introduce a model that enables the exploration of gas exchange during oscillatory ventilation with generalized frequency content.

Computational simulations of ventilation distribution in one-dimensional branching structures demonstrate strong frequency-dependence of heterogeneity (1, 17). These findings reflect the importance not only of local mechanical properties, but also of the network geometry that connects individual airways and acinar structures. However, the distribution of oscillatory flows alone is not sufficient for the prediction of overall gas exchange, and thus a model of gas transport must be developed for this purpose.

We intend to use this model as a theoretical framework for predicting the efficacy of oscillatory ventilator waveforms under physiologically relevant conditions. Our hypothesis is that optimal oscillatory ventilation provides uniform distribution of oscillatory flow. Support for this hypothesis is found in previous studies of high frequency percussive ventilation (HFPV), which involves the superposition of HFOV and conventional mechanical ventilation (42, 58). HFPV improved gas exchange and ventilation-perfusion matching compared to either CMV or HFOV alone in case studies of certain pathologies, including ARDS (16, 22, 47, 72, 85). Further study into the optimization of this strategy has been very limited, and HFPV has not demonstrated improved mortality in ARDS. This lack of improved mortality may be related to the reliance on large tidal volumes at low frequencies. Thus, a systematic and quantitative approach to the design of ventilation comprising optimized frequency content is warranted.

2. METHODS

2.1. VENTILATION DISTRIBUTION IN AN ANATOMIC MODEL

2.1.1. Overview

We model the airway tree as a network of spatially oriented airway segments, with sizes and positions based on segmented airways from three-dimensional computed tomographic (3DCT) scans. Airway dimensions and wall properties define longitudinal and shunt impedances, under the assumption of Womersley-type oscillatory flow (103). Every terminal airway segment ends in an acinus, modeled with constant phase impedance. Mechanical properties for each airway and acinus are related to individual transmural or transpulmonary pressures, calculated as the difference between pressure inside the airway or acinus and the local pleural pressure (P_{pl}). Pleural pressure is defined by the gravitational gradient across the span of the lung. For simulations of high frequency oscillations with small tidal volumes, the effects of intratidal variations in mechanical properties are not considered, including processes of cyclic recruitment and overdistension. Ventilation distribution is computed as a steady-state process in the frequency domain (17).

2.1.2. Airways

Airway dimensions are extracted from 3DCT scans of dog lungs (52), for airways large enough to be detected and segmented. Smaller airways are generated algorithmically, using a space-filling model of airway network topology

(90). Figure 5 shows an example of the segmented central airways and generated airway network.

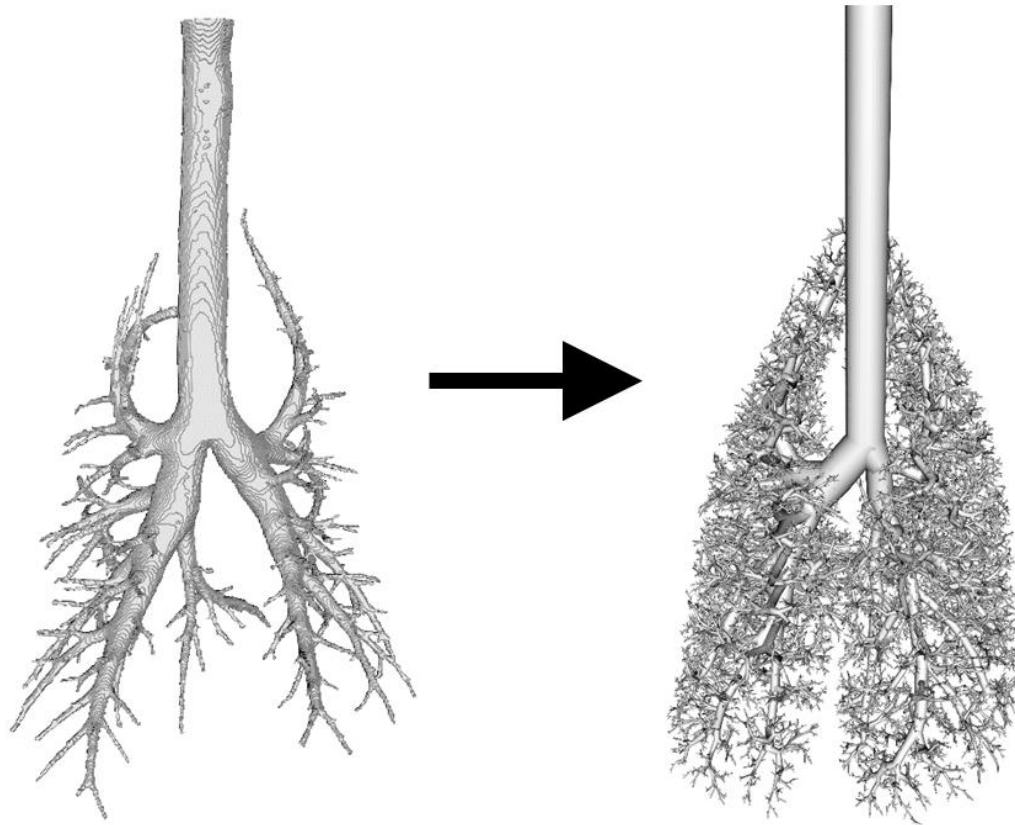


Figure 5. Segmented central airways from 3DCT scan of 25 kg dog at 30 cmH₂O distending pressure (left) and generated network of cylinders used in computational model (right).

Relationships for airway wall thickness, cartilage content, and generation/order are extrapolated from Horsfield generations (17, 40, 60), using the inner radius as the independent variable. Airway impedance is modeled with longitudinal and shunt components (17). The longitudinal impedance is calculated assuming Womersley-type oscillatory flow in cylindrical tubes (95, 103). The relative contributions of resistance and inertance to the longitudinal impedance are determined by the Womersley number α_w , which was defined in

Equation 11 in terms of airway radius r , angular frequency of oscillation ω , air density ρ , and air dynamic viscosity μ . Longitudinal impedance is the calculated by Equation 13, where J_0 and J_1 are Bessel functions of the first kind of orders 0 and 1, respectively, and L is the length of the cylindrical airway segment.

$$Z_{\text{long}} = \left(\frac{j\omega\rho L}{\pi r^2} \right) \left[1 - \frac{2J_1(\alpha_W\sqrt{-j})}{(\alpha_W\sqrt{-j})J_0(\alpha_W\sqrt{-j})} \right]^{-1} \quad \text{Equation 13}$$

The shunt impedance comprises the parallel shunt pathways of gas compression and wall distension (17). Gas compression is modeled as an elastic element in accordance with Boyle's law, defined by the ratio of absolute pressure inside a segment and the segment's volume. Wall distension is partitioned into parallel soft (subscript s) and cartilaginous (subscript c) tissue compartments, with each subdivided into series resistive (R), inertial (I), and elastic (C) components. The shunt impedance is calculated according to Equation 14, with gas compression compliance C_g defined by Equation 15 in terms of segment volume V_{seg} and absolute distending pressure P_{seg} .

$$Z_{\text{shu}} = \left[\frac{1-F_c}{R_s+j\omega I_s+(j\omega C_s)^{-1}} + \frac{F_c}{R_c+j\omega I_c+(j\omega C_c)^{-1}} + C_g \right]^{-1} \quad \text{Equation 14}$$

$$C_g = \frac{V_{\text{seg}}}{P_{\text{seg}}} \quad \text{Equation 15}$$

The orientation of mechanical impedance elements considered in this model of an airway segment is presented in Figure 6.

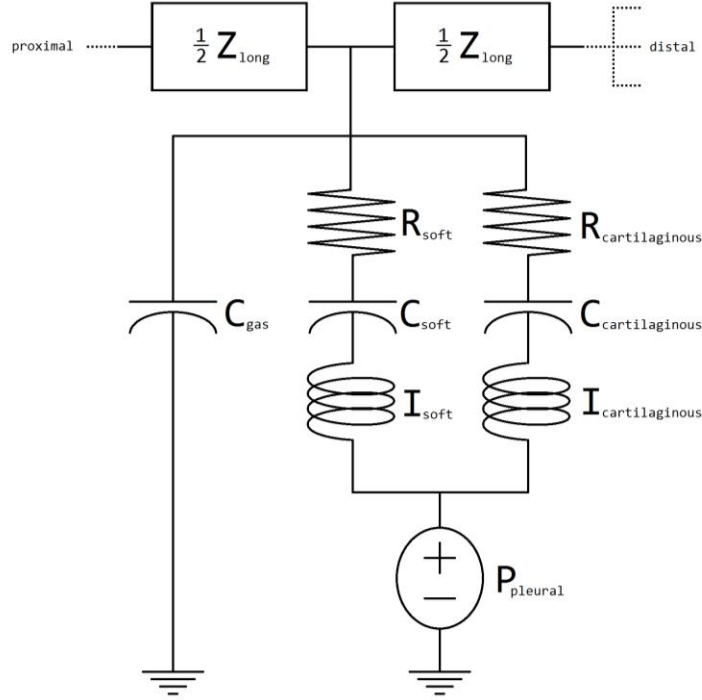


Figure 6. Circuit representation of an airway segment element. Input flow at the proximal node is divided between parallel shunt pathways of gas compression and wall distension, and the subtending airway subtrees at the distal node. Equations Equation 13 and Equation 14 provide the impedance for Z_{long} and Z_{shu} , respectively.

2.1.3. Acini

The acini are modeled as point elements at the distal centerpoints of terminal airway segments, with volume and surface area. The impedance of acini (Z_{acn}) to input flow is governed by a constant phase model, which incorporates a tissue damping (G) and elastance (H) parameters, the ratio of which defines the hysteresivity ($\eta = \frac{G}{H}$).

$$Z_{acn} = \left[\left(\frac{(\eta - j)H_n}{\omega^\alpha} \right)^{-1} + j\omega C_g \right]^{-1} \quad \text{Equation 16}$$

$$\alpha = \frac{2}{\pi} \tan^{-1} \left(\frac{1}{\eta} \right) \quad \text{Equation 17}$$

The constant phase model accurately reflects the power-law nature of the pressure-volume relationship in the respiratory system (41, 88). H and η are determined by empirical functions of transpulmonary pressure P_{tp} (56). Although $H(P_{tp})$ and $\eta(P_{tp})$ were fit to data based on whole-lung impedance measurements in dogs, they are applied in this model to individual acini under the assumption that acinar mechanics were relatively homogeneous under the measurement conditions. The impedance measurements were calculated based on the difference between airway opening pressure and esophageal pressure (approximating pleural pressure). Therefore in application to individual acini, $H(P_{tp})$ and $\eta(P_{tp})$ are functions of transpulmonary pressure, between the pressure inside the acinus P_{acn} and the local pleural pressure P_{pl} . The orientation of mechanical impedance elements considered in this model of an acinus is presented in Figure 7.

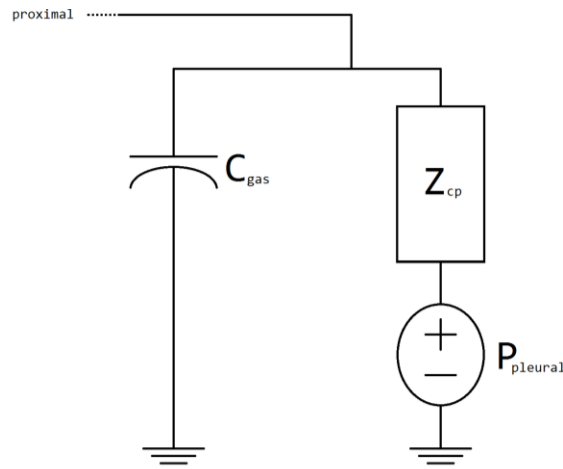


Figure 7. Circuit representation of an acinar element. Input flow at the proximal node is divided between parallel pathways of gas compression compliance and acinar volume expansion, whose impedance is modeled by a constant phase element described in equations Equation 16 and Equation 17.

2.1.4. Pleural Pressure

Regional pleural pressure in the model is defined according to a spatially-oriented gravitational gradient. Ventilation is driven by pressure changes at the airway opening rather than pressure changes in the pleural space, simulating mechanical ventilation in a sedated patient. Accordingly, temporal variations in pleural pressure are not accounted for, aside from pressure variations due to changes in position. Expansion of the lung at higher mean airway pressures causes an increase in the spread of pleural pressures due to the gravitational gradient. However, at any given mean airway pressure, intratidal variations in airway sizes and positions are neglected, and therefore the pleural pressure is modeled as a spatially-varying temporally-constant independent pressure source.

2.1.5. Injury

Heterogeneous injury is simulated by modulating acinar tissue elastance H according to a gravitationally-weighted gradient noise distribution. Gradient noise, created using the Perlin method (23), produces a textured distribution that is smoother and more natural than random value noise. Gravitational weighting increases the magnitude of the noise distribution towards the dependent regions, which mimics the effect of fluid accumulation in ARDS-affected lungs. Although the resulting elastance distribution does not accurately mimic the pathophysiologic effects of ARDS on tissue mechanics of parenchyma, it suffices as a simple approximation of heterogeneous mechanics. The elastance of each acinus is assumed constant, which does not mimic intra-tidal changes in

mechanics due to overdistension and recruitment/derecruitment. This injury model does not affect the mechanics or size of the airways, and therefore is unrealistic in simulation of injury, yet conveniently allows comparison of gas transport through identical airway network geometry under variable ventilation distribution determined exclusively by differences in acinar mechanics.

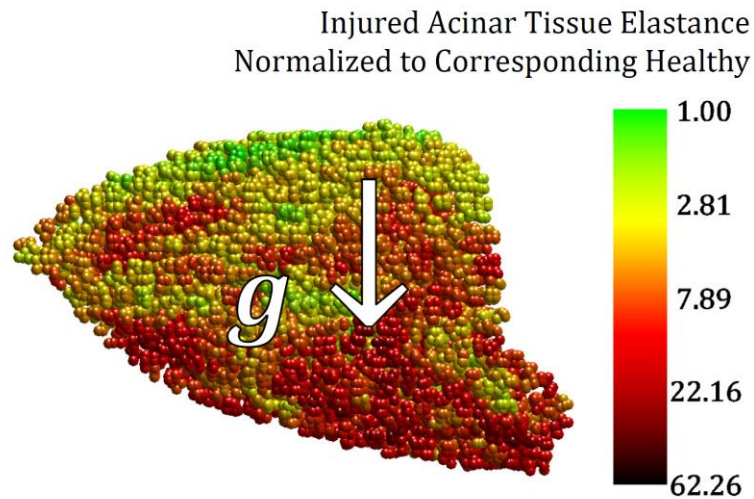


Figure 8. Heterogeneous lung injury is simulated by scaling tissue elastance according to gravitationally-weighted gradient noise, which produces a cloudy, heterogeneous texture. The color of each acinar element corresponds to the ratio of tissue elastance $H_{\text{injured}}/H_{\text{healthy}}$. The direction of gravitational force (g) is indicated by the arrow.

2.1.6. Impedance

The impedance of the entire airway tree, as well as that of each subtree, is necessary to determine the distribution of flow. Each subtree, given by the parent airway segment and all distal children, can be recursively traversed using Equation 18; at each parent segment, the total impedance of the subtree (Z_{sub}), inclusive of the parent, is calculated by adding in series the impedance of the

parent segment with the parallel combination of all children segments' subtree impedances ($Z_{\text{sub,child}(n)}$).

$$Z_{\text{sub}} = \frac{1}{2}Z_{\text{long}} + \left[\left(\frac{1}{2}Z_{\text{long}} + [\sum_n Z_{\text{sub,child}(n)}^{-1}]^{-1} \right)^{-1} + Z_{\text{shu}}^{-1} \right]^{-1} \quad \text{Equation 18}$$

As illustrated in Figure 6, the parent contains a parallel shunt impedance Z_{shu} bisecting the longitudinal impedance Z_{long} , which includes a pressure source accounting for P_{pl} . However, P_{pl} can be safely ignored in the frequency domain impedance calculations as a constant independent pressure source.

2.1.7. Ventilation distribution

Given a known flow oscillation at the proximal end of a parent airway segment \dot{V}_{prox} , the flow oscillations at the shunt \dot{V}_{shu} , at the distal end of the parent airway segment \dot{V}_{dist} , and at the proximal end of each n^{th} child airway segment $\dot{V}_{\text{prox,child}(n)}$ are computed from the current division between parallel pathway impedances (17).

$$\dot{V}_{\text{shu}} = \dot{V}_{\text{prox}} \left[\frac{\frac{1}{2}Z_{\text{long}} + [\sum_n Z_{\text{sub,child}(n)}^{-1}]^{-1}}{\frac{1}{2}Z_{\text{long}} + [\sum_n Z_{\text{sub,child}(n)}^{-1}]^{-1} + Z_{\text{shu}}} \right] \quad \text{Equation 19}$$

$$\dot{V}_{\text{dist}} = \dot{V}_{\text{prox}} - \dot{V}_{\text{shu}} \quad \text{Equation 20}$$

$$\dot{V}_{\text{prox,child}(m)} = \dot{V}_{\text{dist}} \left[\frac{[\sum_n Z_{\text{sub,child}(n)}^{-1}]^{-1}}{Z_{\text{sub,child}(m)}} \right] \quad \text{Equation 21}$$

Applied to all branches of the airway network, the resulting ventilation distribution is computed in the frequency domain, with a complex value for each frequency representing the magnitude and phase relative to the input flow at the airway opening. For the purposes of simplicity, these calculations are performed with an input flow at the airway opening with unity magnitude and zero phase at all frequencies. Linearity and time invariance are assumed when computing ventilation distribution *via* mechanical impedance; thus it is also assumed that the input flow at the airway opening can be assigned any complex scalar, and the ventilation distribution scales linearly. This assumption is valid only for small amplitudes of oscillation, such that the mechanical properties of the respiratory system do not change significantly over the period of oscillation.

2.1.8. Personal Dead Space

Gas transport during ventilation with large tidal volumes is affected by the dead space volume V_D of the respiratory system in a manner consistent with Equation 1. However, this relationship only applies to total CO_2 elimination, and furthermore assumes a uniform distribution of ventilation, such that Equation 1 is most appropriate for a single compartment model of the respiratory system. In order to properly model the mechanism of direct alveolar ventilation, we must consider the effects of the ventilation distribution on the amounts of fresh gas and dead space gas entering each individual acinar compartment during one period of oscillation. To achieve this, we apply the concept of “personal dead space” used by Fortune and Wagner to describe the non-uniform distribution of

airway segment volumes to the terminal acini (28). The fraction of proximal dead space V_D^* which oscillates through a child $V_{D,\text{child}(m)}^*$ of a particular parent airway segment is calculated in proportion to the flow division between that child and the other children, as shown in Equation 25:

$$V_{D,\text{child}(m)}^* = [V_D^* + V_{\text{seg}}] \left[\frac{\dot{V}_{\text{prox,child}(m)}}{\dot{V}_{\text{dist}}} \right] \quad \text{Equation 22}$$

In this manner, the dead space of all conducting airways is successively distributed in proportion to the ventilation distribution through subtending airways until reaching the terminal acini. The effect of direct alveolar ventilation for a particular acinar compartment can then be determined by comparing V_D^* for that acinus to the total volume delivered to that acinus over one period of oscillation.

2.2. GAS TRANSPORT DURING OSCILLATORY FLOW

2.2.1. Transport Resistance in Branching Network

At steady state, the solution of one-dimensional molecular diffusion in a tube with a concentration gradient $\Delta\bar{c}$ across the length L of the tube is a linear axial profile of concentration, with molar flux \dot{M} in the axial direction proportional to the concentration gradient as given by Fick's law:

$$\dot{M} = -\pi r^2 D_{\text{mol}} \frac{\Delta\bar{c}}{L} \quad \text{Equation 23}$$

The case of one-dimensional steady state diffusion in a tube can be recast as a circuit analog, with partial pressure gradient Δp driving the molar flux through a linear transport resistance R_T , as defined in Equation 24 and Equation 25:

$$\dot{M} = -\frac{1}{R_T} \Delta p \quad \text{Equation 24}$$

$$R_T = \frac{R_{\text{gas}} T L}{\pi r^2 D_{\text{mol}}} \quad \text{Equation 25}$$

where R_{gas} is the universal gas constant and T is the absolute temperature, assuming ideal gas behavior. Because of the simplicity and ease of solving systems of linear ordinary differential equations, this approach is favorable in the context of a large number of branching airways. A mesh analysis of the system of equations ensures conservation of mass, such that the sum of molar fluxes at the airway opening and every terminal airway segment is zero. The molar fluxes at the proximal node of every acinus are chosen as state variables, and the system of equations is expressed in matrix notation as:

$$\mathbf{R}_T \dot{\mathbf{M}} = \Delta \mathbf{p} \quad \text{Equation 26}$$

where each row of the system corresponds to the mass flux from a single acinus to the airway opening. For example, given the simple bifurcating system shown in Figure 9, using mesh analysis forms the system of equations with matrices:

$$\mathbf{R}_T = \begin{bmatrix} R_{T_0} + R_{T_1} & R_{T_0} & R_{T_0} \\ R_{T_0} & R_{T_0} + R_{T_2} + R_{T_3} & R_{T_0} + R_{T_2} \\ R_{T_0} & R_{T_0} + R_{T_2} & R_{T_0} + R_{T_2} + R_{T_4} \end{bmatrix} \quad \text{Equation 27}$$

$$\dot{\mathbf{M}} = \begin{bmatrix} \dot{M}_{acn,1} \\ \dot{M}_{acn,2} \\ \dot{M}_{acn,3} \end{bmatrix} \quad \text{Equation 28}$$

$$\Delta \mathbf{p} = \begin{bmatrix} p_{acn,1} - p_{ao} \\ p_{acn,2} - p_{ao} \\ p_{acn,3} - p_{ao} \end{bmatrix} \quad \text{Equation 29}$$

Accordingly, each term in $\Delta \mathbf{p}$ corresponds to total partial pressure loss between an acinus and the airway opening $p_{acn,i} - p_{ao}$, and each row of the matrix product of \mathbf{R}_T and $\dot{\mathbf{M}}$ corresponds to the sum of partial pressure losses due to transport resistance in each airway between that acinus and the airway opening.

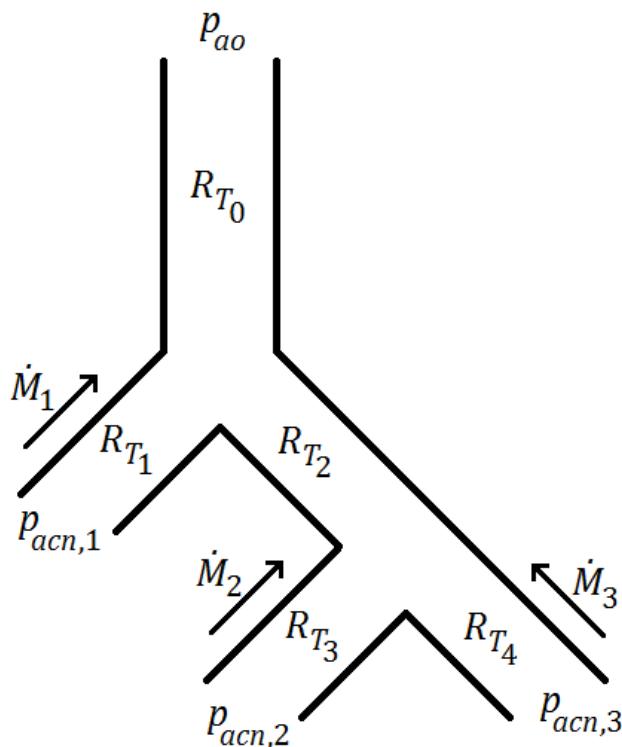


Figure 9. Simplified representation of transport resistances in a model bifurcation and the corresponding system of linear equations representing the mesh analysis approach to solving for molar fluxes.

The matrix of coefficients \mathbf{R}_T is completely full because the transport resistance of the trachea is included in every mesh. Therefore memory costs may be substantial for large numbers of airways. An alternative to mesh analysis is nodal analysis, which involves choosing the state variables as the partial pressures at every proximal node. Nodal analysis forms a system of equations using conservation of mass flux applied to each individual node, which produces

a coefficient matrix far sparser than that of mesh analysis. However, small numerical inaccuracies at each node can result in substantial discrepancies between the flux at the airway opening and the total flux across the acini. Thus, mesh analysis is preferred.

2.2.2. Diffusive/Dispersive Transport Resistance

The case of steady state dispersion, after a long period of unsteady oscillatory flow, can be simplified to enhanced diffusion along a linear concentration gradient. The diffusive transport resistance R_T^{diff} is modified from Equation 25 with an effective diffusivity D_{eff} rather than the molecular diffusivity D_{mol} . D_{eff} , as described in 1.1.3, comprises the sum of D_{mol} and $D_{\text{dis}}^{\text{osc}}$, where D_{dis} is a frequency-dependent enhancement to D_{eff} that results from the velocity profile distortions during oscillatory flow (2).

$$D_{\text{eff}} = D_{\text{mol}} + D_{\text{dis}}^{\text{osc}} \quad \text{Equation 30}$$

During single frequency oscillatory ventilation, the value of $D_{\text{dis}}^{\text{osc}}$ for any individual airway depends on only a single frequency and amplitude of oscillation, as given by Equation 9. The function β_2 in Equation 9 is derived directly from Watson 1983, and is a function of both α_W and Sc involving Kelvin functions of α_W and their derivatives (101).

During oscillation with multiple simultaneous frequencies, the value of $D_{\text{dis}}^{\text{osc}}$ is equal to the sum of dispersion coefficients computed for each frequency individually. This finding can be derived from a brief analysis following the same structure presented in Watson 1983 (101).

Consider the flow in a tube with oscillatory velocity

$$u = \sum_i \Re\{U_i(x, y)e^{j\omega_i t}\} \quad \text{Equation 31}$$

where $U_i(x, y)$ is a velocity amplitude distribution over the cross-section in the x - y plane and is periodic in time t with angular frequency ω_i . The operator $\Re\{\cdot\}$ indicates the real part of the complex-valued argument within the brackets. Consider contaminant concentration

$$c = -\gamma z + \sum_i \Re\{\gamma\theta_i(x, y)e^{j\omega_i t}\} \quad \text{Equation 32}$$

where z is the axial direction, γ is a constant, and $\theta_i(x, y)$ is related to a concentration amplitude distribution over the cross-section in the x - y plane and is periodic in time t with angular frequency ω_i . The rate of flux of the contaminant has advective and diffusive terms integrated over the area of the cross section A_{cs} , given by

$$\begin{aligned} \iint_{A_{cs}} \left[uc - D_{\text{mol}} \frac{\partial c}{\partial z} \right] dA = & \quad \text{Equation 33} \\ \iint_{A_{cs}} \left[\gamma D_{\text{mol}} + \frac{1}{2} \left\{ \sum_i (U_i e^{j\omega_i t} + \bar{U}_i e^{-j\omega_i t}) \right\} \left(-\gamma z \right. \right. \\ & \left. \left. + \frac{1}{2} \gamma \left\{ \sum_i (\theta_i e^{j\omega_i t} + \bar{\theta}_i e^{-j\omega_i t}) \right\} \right) \right] dA \end{aligned}$$

where bars denote complex conjugates. The mean rate of flux, averaged over time, is

$$\iint_{A_{cs}} \left[\gamma D_{\text{mol}} + \frac{1}{4} \gamma \left\{ \sum_i (U_i \bar{\theta}_i + \bar{U}_i \theta_i) \right\} \right] dA \quad \text{Equation 34}$$

wherein all oscillatory terms after expansion (i.e. terms preceding $e^{j\omega_i t} e^{j\omega_i t}$ or preceding $e^{j\omega_i t} e^{-j\omega_k t}$ with $i \neq k$) of the multiplication are reduced to zero in the time-averaging, and only the time-independent terms (i.e. terms preceding $e^{j\omega_i t} e^{-j\omega_i t}$) remain. The effective diffusivity is

$$D_{\text{eff}} = D_{\text{mol}}(1 + \mathcal{R}) \quad \text{Equation 35}$$

where \mathcal{R} is the relative increase in diffusivity over molecular diffusivity given by

$$\mathcal{R} = \frac{1}{4D_{\text{mol}}A_{\text{cs}}} \iint_{A_{\text{cs}}} \left[\sum_i (U_i \bar{\theta}_i + \bar{U}_i \theta_i) \right] dA \quad \text{Equation 36}$$

which rearranges to

$$\mathcal{R} = \sum_i \left(\frac{1}{4D_{\text{mol}}A_{\text{cs}}} \iint_{A_{\text{cs}}} [U_i \bar{\theta}_i + \bar{U}_i \theta_i] dA \right) \quad \text{Equation 37}$$

and the term inside the summation on the right side is identical to the relative increase for any individual frequency of oscillation (101). Thus the overall diffusive/dispersive transport resistance R_T^{diff} is given by:

$$R_T^{\text{diff}} = \frac{R_{\text{gas}} TL}{\pi r^2 [D_{\text{mol}} + \sum_i D_{\text{dis}}^{\text{osc}}(f_i)]} \quad \text{Equation 38}$$

This conclusion relies on the reduction of time-averaged $e^{2j\omega_i t}$ and $e^{j(\omega_i - \omega_k)t}$ terms to zero over a long period of oscillation in the transition from Equation 33 to Equation 34. Therefore, this model of dispersion during simultaneous multiple frequencies may not apply when the beat frequency (i.e. the difference between any two frequencies) is very small.

Turbulent dispersion was modeled according to the method of Fredberg in 1980 (29). This method assumed a quasi-steady approximation for turbulent

flows, i.e., that flow oscillations are slow compared to the time scale of turbulent eddies. Therefore, the dispersion coefficient is averaged over the period of oscillation, using the root-mean-square value of mean axial velocity \bar{U} in Equation 8, such that:

$$D_{\text{dis}}^{\text{turb}} = \bar{U}_{RMS} r \cdot \beta_1(\text{Re}) \quad \text{Equation 39}$$

Further, the value of $\beta_1(\text{Re})$ is approximated as a constant ϵ with a unity order of magnitude. The specific value of $\epsilon = 0.725$ used in the present model was derived from Scherer et al., averaging between the experimentally derived values for inspiratory and expiratory flows (78, 80). Finally, Equation 39 is only valid during turbulent flows: this was represented in the model using a critical Reynolds number $\text{Re}_{\text{crit}} = 30$ to determine the transition from laminar to turbulent flows (50, 80). Equations for oscillatory dispersion (i.e. Equation 9 and Equation 38) were applied to define R_T^{mix} in airways with $\text{Re} < \text{Re}_{\text{crit}}$; equations for turbulent dispersion (i.e. Equation 39) were used to define R_T^{mix} in airways with $\text{Re} \geq \text{Re}_{\text{crit}}$.

The complete formulation of diffusive and dispersive transport resistance is:

$$R_T^{\text{diff}} = \frac{R_{\text{gas}} TL}{\pi r^2 D_{\text{eff}}} \quad \text{Equation 40}$$

where

$$D_{\text{eff}} = \begin{cases} D_{\text{mol}} + \sum_i D_{\text{dis}}^{\text{osc}}(f_i) & , \quad \text{Re} < \text{Re}_{\text{crit}} \\ D_{\text{mol}} + D_{\text{dis}}^{\text{turb}} & , \quad \text{Re} \geq \text{Re}_{\text{crit}} \end{cases} \quad \text{Equation 41}$$

One important limitation of this model is found in its derivation for oscillations in infinitely long tubes. Enhanced diffusion *via* dispersion is not

sufficient for describing transport in a branching network. Oscillations of flow at bifurcations result in increased mixing of gases that diffusive transport resistance alone cannot describe (76–78).

2.2.3. *Mixing Transport Resistance*

In general, when the amplitude of volume flux through an airway segment exceeds the segment's volume, the impact of convective mixing at bifurcations must be considered. To approach this problem, we consider a tube with volume V_{seg} and fixed concentrations of a certain gas at either end of the tube, as shown in Figure 10.

The opposing ends of the tube can be thought of as infinitely large reservoirs with complete and immediate mixing of incoming flow. The net molar flux through the tube $\dot{M} = \frac{dn}{dt}$, where n is moles of gas and $n = cV$, is given by the oscillatory volume magnitude V_{osc} and frequency of oscillation:

$$\dot{M} = \begin{cases} [c_1(V_{\text{osc}} - V_{\text{seg}})f] - [c_2(V_{\text{osc}} - V_{\text{seg}})f] & , V_{\text{osc}} > V_{\text{seg}} \\ 0 & , V_{\text{osc}} \leq V_{\text{seg}} \end{cases} \quad \text{Equation 42}$$

which reduces to:

$$\dot{M} = \begin{cases} [c_1 - c_2][(V_{\text{osc}} - V_{\text{seg}})f] & , V_{\text{osc}} > V_{\text{seg}} \\ 0 & , V_{\text{osc}} \leq V_{\text{seg}} \end{cases} \quad \text{Equation 43}$$

Assuming ideal gas behavior, the concentration can be related to partial pressure:

$$c_{\text{gas}} = \frac{n_{\text{gas}}}{V_{\text{total}}} = \frac{F_{\text{gas}}n_{\text{total}}}{V_{\text{total}}} = \frac{F_{\text{gas}}p_{\text{total}}}{R_{\text{gas}}T} = \frac{p_{\text{gas}}}{R_{\text{gas}}T} \quad \text{Equation 44}$$

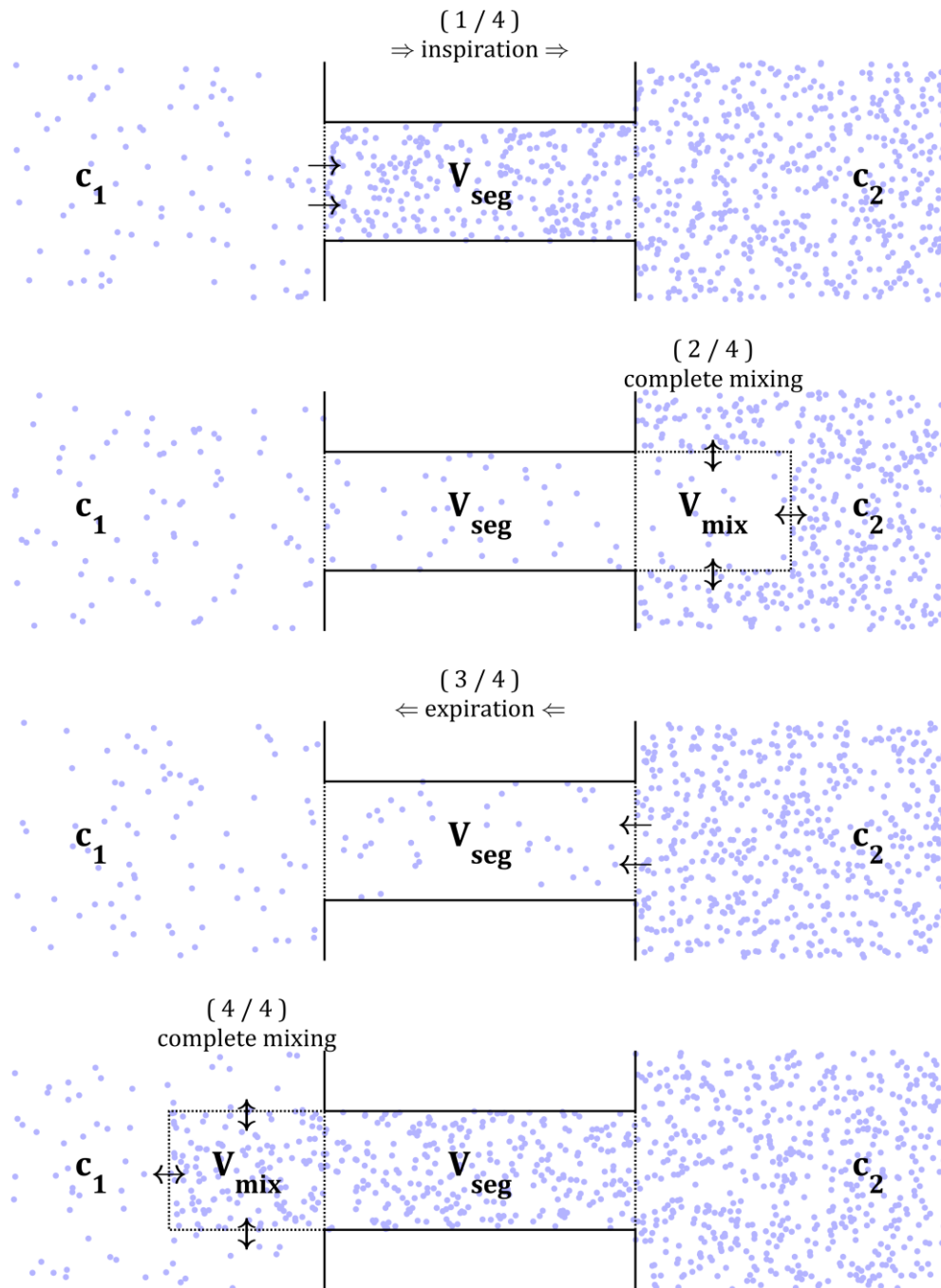


Figure 10. Model of an airway segment with reservoirs at either end containing the same gas species at different concentrations (color used only to clarify different concentrations – color does not indicate different species). A volume of gas is oscillated through the segment, and the volume of gas that passes completely through the segment is available for mixing with the opposing reservoir.

We can relate concentrations in Equation 43 to partial pressures:

$$\dot{M} = \begin{cases} \left[\frac{p_1 - p_2}{R_{\text{gas}} T} \right] [(V_{\text{osc}} - V_{\text{seg}}) f] & , V_{\text{osc}} > V_{\text{seg}} \\ 0 & , V_{\text{osc}} \leq V_{\text{seg}} \end{cases} \quad \text{Equation 45}$$

and we get the result:

$$\dot{M} = \begin{cases} \Delta p \left[\frac{(V_{\text{osc}} - V_{\text{seg}}) f}{R_{\text{gas}} T} \right] & , V_{\text{osc}} > V_{\text{seg}} \\ 0 & , V_{\text{osc}} \leq V_{\text{seg}} \end{cases} \quad \text{Equation 46}$$

from which it is evident that the mixing transport resistance is:

$$R_T^{\text{mix}} = \frac{\Delta p}{\dot{M}} = \frac{R_{\text{gas}} T}{f V_{\text{mix}}} \quad \text{Equation 47}$$

where

$$V_{\text{mix}} = \begin{cases} V_{\text{osc}} - V_{\text{seg}} & , V_{\text{osc}} > V_{\text{seg}} \\ 0 & , V_{\text{osc}} \leq V_{\text{seg}} \end{cases} \quad \text{Equation 48}$$

This expression for mixing transport resistance is similar in form to Equation 1, which defined the proportionality of CO₂ elimination and the rate of alveolar ventilation during gas exchange dominated by bulk advection. Note that $R_T^{\text{mix}} = \infty$ when $V_{\text{mix}} = 0$, implying that no transport occurs due to advection (regardless of concentration gradient) when the volume amplitude is small such that gas at one node does not oscillate past the adjacent node during the period of an oscillation. There are a few important assumptions involved in this definition of mixing transport resistance:

- (1) Bulk flow – such that the contribution from any one node is proportional to the difference between the oscillatory volume and segment volume, regardless of the shape of the velocity profile. This assumption also leads

directly to the corollary assumption that there is zero mixing transport between two nodes if $V_{osc} < V_{seg}$.

- (2) Complete mixing of V_{mix} – such that gas which does oscillate from one node past a neighboring node (according to the first assumption) mixes completely and immediately.

Generalization of this definition of mixing transport resistance to multiple frequencies requires a nonlinear approach, because the value of V_{mix} varies in time depending on the amplitudes and phases of superimposed oscillations. Applying the same concept requires the generalization of V_{mix} over the full period of a broadband waveform, using the fundamental frequency f_0 rather than f .

In this case, V_{mix} can be described by the sum of gas volumes that oscillate past the adjacent node over the duration of one full period. Replacing f with f_0 in Equation 48, we get:

$$R_T^{mix} = \frac{\Delta p}{\dot{M}} = \frac{R_{gas}T}{f_0 V_{mix}} \quad \text{Equation 49}$$

where V_{mix} is more generally redefined as:

$$V_{mix} = \int_0^{\frac{1}{f_0}} \dot{V}_{mix}^*(t) dt \quad \text{Equation 50}$$

The limit of integration $\frac{1}{f_0}$ is determined by the period of the greatest common factor of the frequencies of oscillation, f_0 (i.e. fundamental frequency). This limit is chosen to ensure that V_{mix} is constant over every period of the fundamental frequency for all time. The flow which contributes to mixing transport $\dot{V}_{mix}^*(t)$,

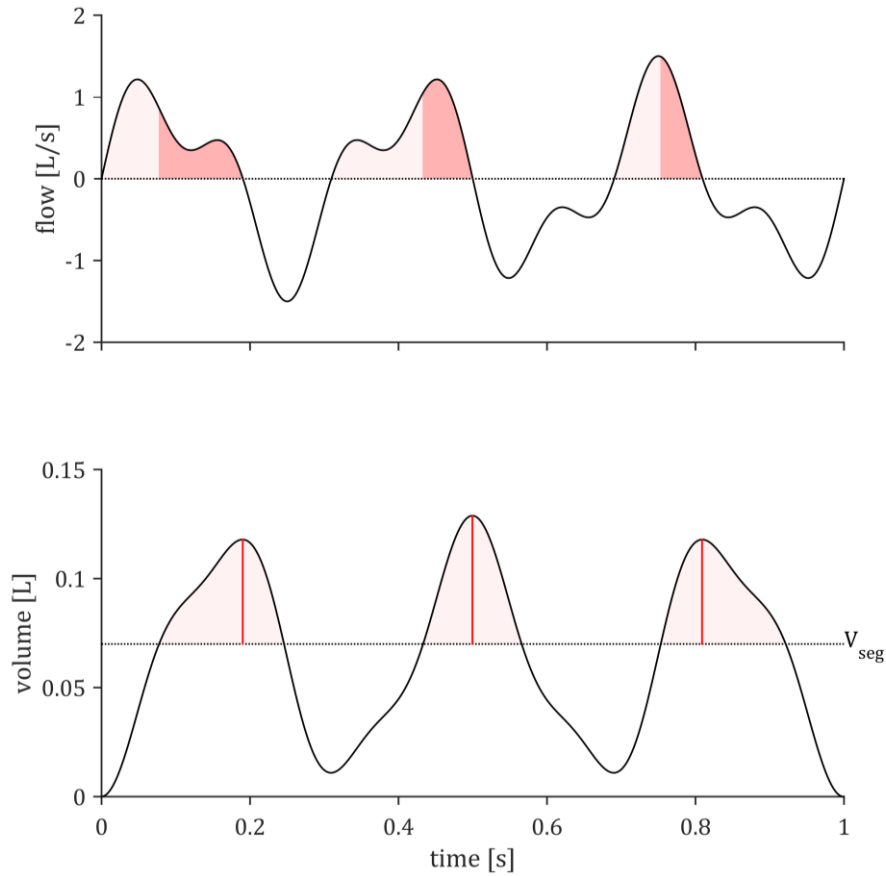


Figure 11. Illustration of method for computing V_{mix} during ventilation with multiple frequencies of oscillation. In this example, two frequencies are used, 3Hz and 7Hz, and $f_0 = 1\text{Hz}$. The light red shading indicates where the conditions of $\dot{V}(t) > 0$ (top) and $V(t) > V_{\text{seg}}$ (bottom) are satisfied. V_{mix} can be calculated in two ways: from the flow integral indicated by dark red shading (where both conditions are satisfied), or from the length of the red lines (i.e. local maxima of $V(t) - V_{\text{seg}}$).

indicated by dark red shading in Figure 11, is given by two conditions (on both oscillatory volume and flow):

$$\dot{V}_{\text{mix}}^*(t) = \begin{cases} \dot{V}(t) & , \quad (V(t) > V_{\text{seg}}) \text{ and } (\dot{V}(t) > 0) \\ 0 & , \quad \text{otherwise} \end{cases} \quad \text{Equation 51}$$

where flow is defined by the sum of sinusoids with individual amplitudes A_i and phases ϕ_i of oscillation:

$$\dot{V}(t) = \sum_i A_i \sin(2\pi f_i t + \phi_i) \quad \text{Equation 52}$$

and volume is defined by the integral of flow:

$$V(t) = \int_0^t \dot{V}(\tau) d\tau \quad \text{Equation 53}$$

The value of V_{mix} is calculated by numerical integration. Note that the numerical integration of this multi-frequency method in the edge case of only one non-zero amplitude A_i produces the same result obtained from the single-frequency method described previously in Equation 47 and Equation 48, and thus the model is consistent.

2.2.4. Total Transport Resistance

The total transport resistance R_T^{tot} is the parallel combination of diffusive and mixing transport resistances.

$$R_T^{\text{tot}} = \frac{1}{\frac{1}{R_T^{\text{diff}}} + \frac{1}{R_T^{\text{mix}}}} = \frac{R_T^{\text{diff}} R_T^{\text{mix}}}{R_T^{\text{diff}} + R_T^{\text{mix}}} \quad \text{Equation 54}$$

Conceptually, R_T^{tot} has an upper limit during zero flow, which is found by taking the limit as R_T^{mix} becomes infinitely large (e.g. when $V_{\text{mix}} = 0$), that results in $R_T^{\text{tot}} = R_T^{\text{diff}}$ with $D_{\text{eff}} = D_{\text{mol}}$.

2.2.5. Direct Alveolar Ventilation

Direct alveolar ventilation occurs when volume amplitudes at the airway opening are sufficiently large such that fresh gas mixes directly with alveolar gas during inspiration. To model this mechanism of gas transport, we will assume

that this volume of fresh gas (V_f) is completely mixed during inspiration and that the same volume of mixed gas is completely removed during expiration, according to the illustration in Figure 12.

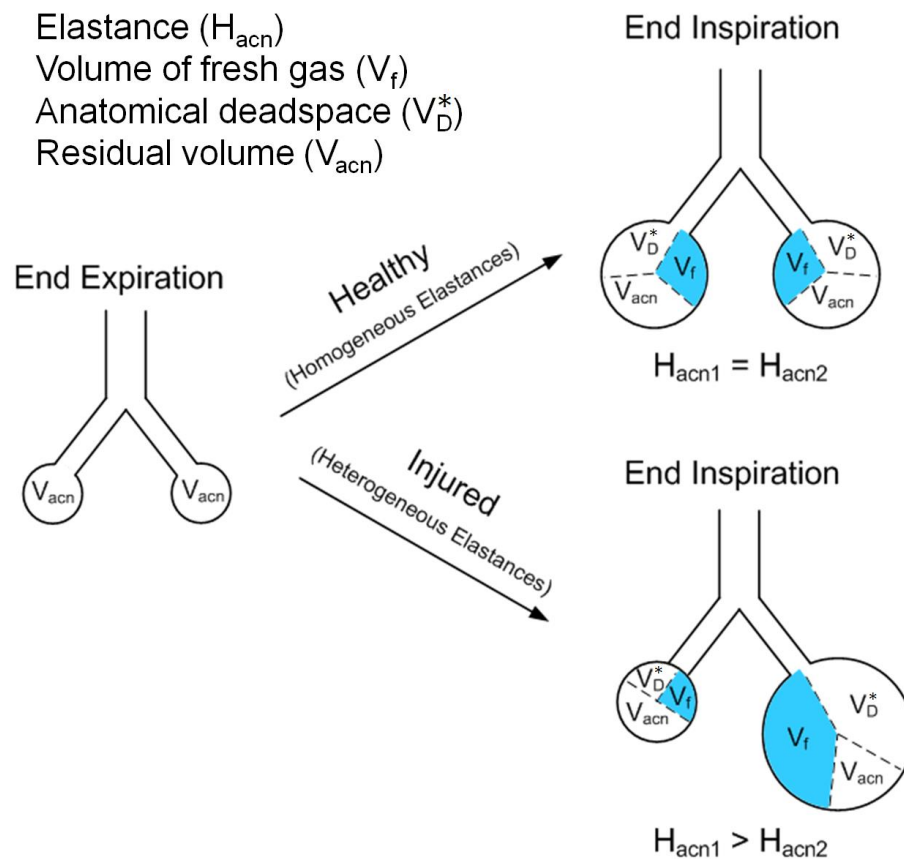


Figure 12. Modeling the distribution of airway segment volumes (i.e. personal dead space, V_D^*) and inspired fresh gas volume (V_f) to each individual acinar compartment. Acini are modeled with tissue elastance and end-expiratory residual volume. Although fresh gas is assumed to have zero pCO_2 , at end-inspiration the gas contents are assumed to be well-mixed. Note that the distribution of inspired volumes is predicted to be non-uniform in the presence of heterogeneous mechanics. Figure reproduced from Colletti *et al.* (18).

The effect of direct alveolar ventilation on gas transport cannot be represented by a transport resistance term. Instead, the amount of CO_2 removed due to direct alveolar ventilation ($\dot{V}_{CO_2}^{DAV}$) is computed directly from $PaCO_2$ and the ventilation distribution (distribution of \dot{V}_{prox} for each acinus), using the concept of

“personal dead space” to apportion an amount of inspired fresh gas to each individual acinus (Section 2.1.8) (28).

$$\dot{V}_{\text{CO}_2}^{DAV} = \frac{\text{PaCO}_2}{863} V_f f \quad \text{Equation 55}$$

where fresh gas volume (V_f) delivered to an acinus is given by:

$$V_f = \begin{cases} \frac{|\dot{V}_{\text{prox}}|}{\pi f} - |V_D^*| & , \quad \frac{|\dot{V}_{\text{prox}}|}{\pi f} > |V_D^*| \\ 0 & , \quad \text{otherwise} \end{cases} \quad \text{Equation 56}$$

The amount of CO_2 elimination computed using these equations to model direct alveolar ventilation is added to the amount of CO_2 elimination computed by solving the matrix of transport resistances (Section 2.2.1). Using this definition of V_f , if the total volume delivered to an acinus over one period of oscillation is less than that acinus’ personal dead space, then there is no contribution of direct alveolar ventilation to CO_2 elimination from that particular acinus.

2.3. LIST OF SIMULATIONS

The mechanical impedance and ventilation distribution were calculated for both healthy and injured conditions, at mean airway pressures 0, 5, 10, 15, and 20 cmH_2O , and at 115 distinct frequencies spanning 0.1 Hz to 100 Hz. However, due to constraints on computational costs as well as the observed similarity of frequency-dependent behavior at varying mean airway pressures, we decided to simulate the gas transport at only one particular mean airway pressure and for a limited range of frequencies.

Gas transport distributions were calculated for both healthy and injured conditions at mean airway pressure 10 cmH₂O, for a wide range of volume amplitudes at each frequency. Each V_T was chosen between 0 mL (zero flow conditions, molecular diffusion only) and 600 mL, with emphasis only on smaller volume amplitudes (i.e. $V_T < V_D$) at higher frequencies. Parameters were chosen as necessary to at least ensure that a simulation representative of eucapnic ventilation was computed at each frequency.

Eucapnic ventilation was determined according to the total CO₂ elimination approximately equal to (i.e. within 5% tolerance of) the predicted \dot{V}_{CO_2} required for eucapnic equilibrium. The selected value $\dot{V}_{CO_2}^{euc} = 1.9 \times 10^{-3} \frac{L}{s}$ was chosen based on average measurements of resting metabolic \dot{V}_{CO_2} per unit body weight in dogs (43), and then adjusting for the weight of the dog (25 kg) from whom CT scans were used to generate this model's airway network.

After simulations of ventilation with a single frequency of oscillation were performed and approximate parameter values for eucapnic ventilation were obtained, gas transport distributions were computed for a selected pair of frequencies, again titrating the volume amplitudes at each frequency to achieve eucapnic ventilation.

3. RESULTS

3.1. MODEL VALIDATION

The first goal, stated in Specific Aim 1, was to validate the computational, by comparing simulated results to experimental data for CO₂ elimination (97) over a wide range of tidal volumes V_T and frequencies f .

Figure 13 shows simulation results for \dot{V}_{CO_2} as a function of V_T and f . Simulation points were chosen for each frequency starting at 0 mL and increasing in increments of 5 mL until \dot{V}_{CO_2} was at least greater than the predicted \dot{V}_{CO_2} required for eucapnic ventilation ($\dot{V}_{CO_2}^{euc}$, Section 2.3). The prediction of $\dot{V}_{CO_2}^{euc}$ is indicated on each plot, as well as the \dot{V}_{CO_2} produced by molecular diffusion only (i.e. zero flow conditions), which establishes the lower bound of gas transport for all values of V_T and f .

There are noticeably different behaviors of the resultant \dot{V}_{CO_2} with respect to V_T and f . In particular, there are certain ranges of volume amplitudes over which some gas transport mechanisms dominate the others: starting from molecular diffusion alone at zero flow conditions, there are dramatic increases in \dot{V}_{CO_2} with the advent of oscillatory dispersion, followed by turbulent dispersion, convective mixing at bifurcations, and finally direct alveolar ventilation. These ranges are indicated in Figure 14.

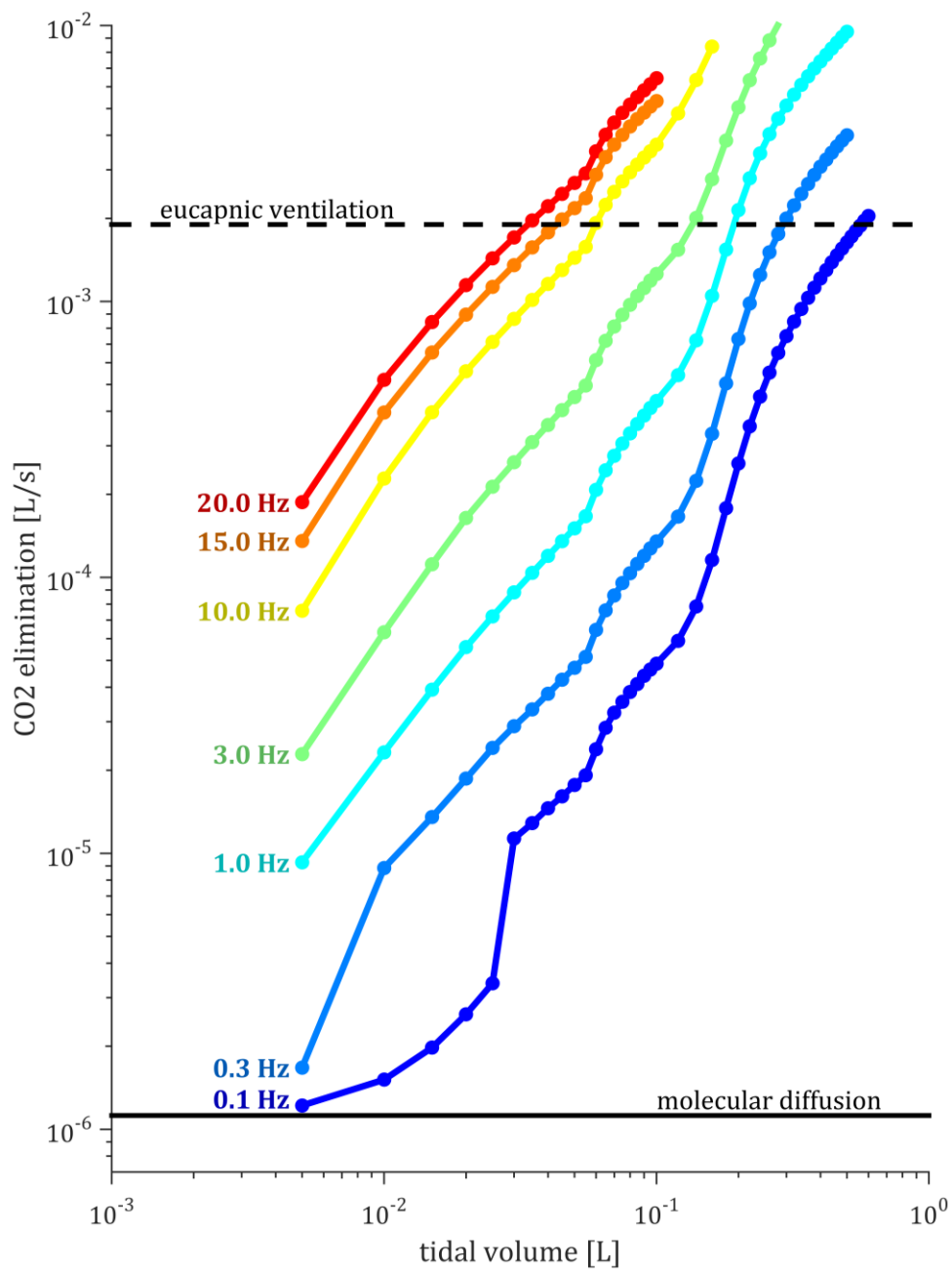


Figure 13. Relationship between \dot{V}_{CO_2} and V_T for a variety of frequencies, each value of f indicated by color. The black lines represent the lower bound of \dot{V}_{CO_2} produced by molecular diffusion alone (zero-flow conditions), and the prediction of required \dot{V}_{CO_2} for eucapnic equilibrium.

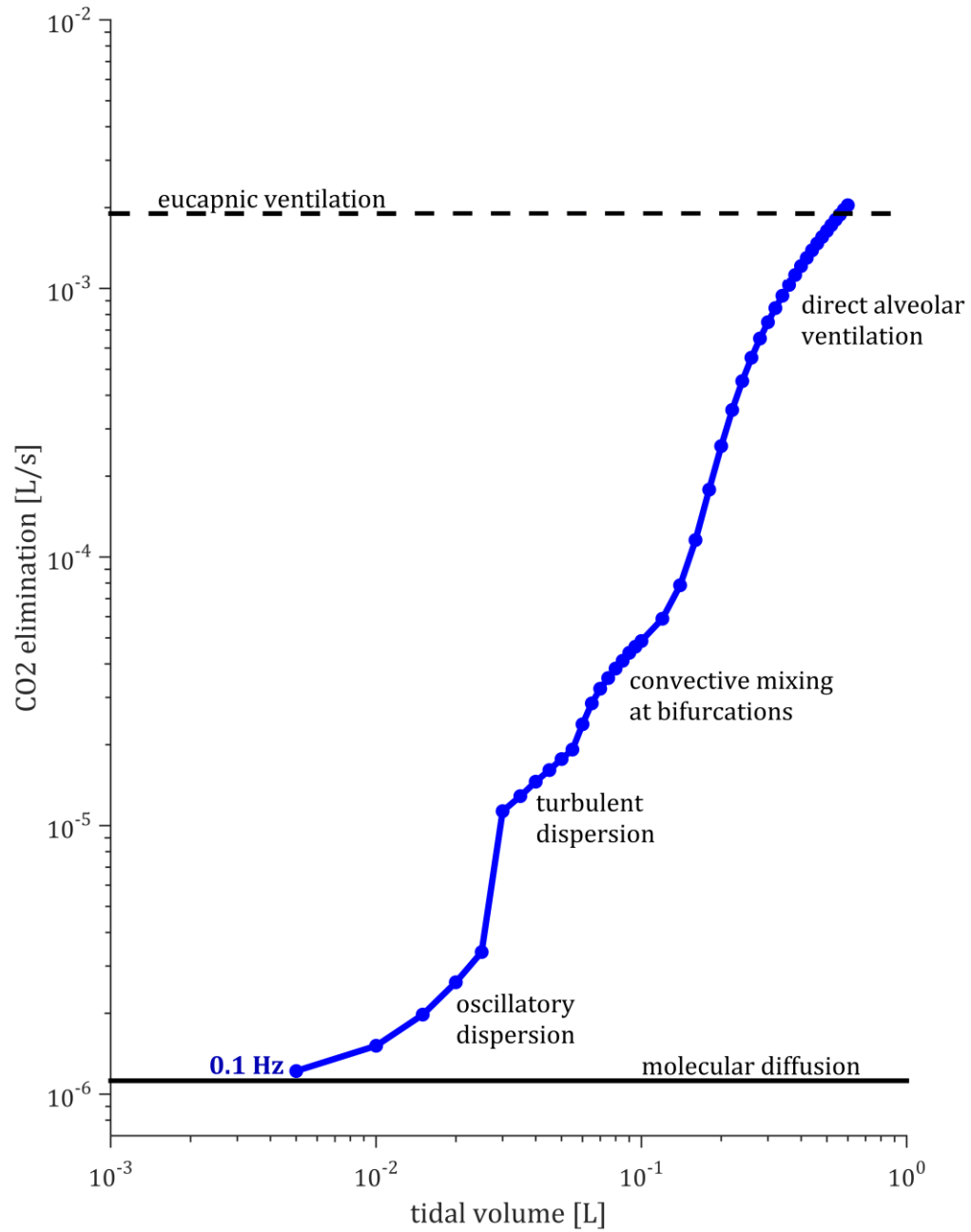


Figure 14. Isolated data of simulations for 0.1 Hz oscillations, with text labels indicating the volume amplitude ranges over which certain gas transport mechanisms dominate overall \dot{V}_{CO_2} .

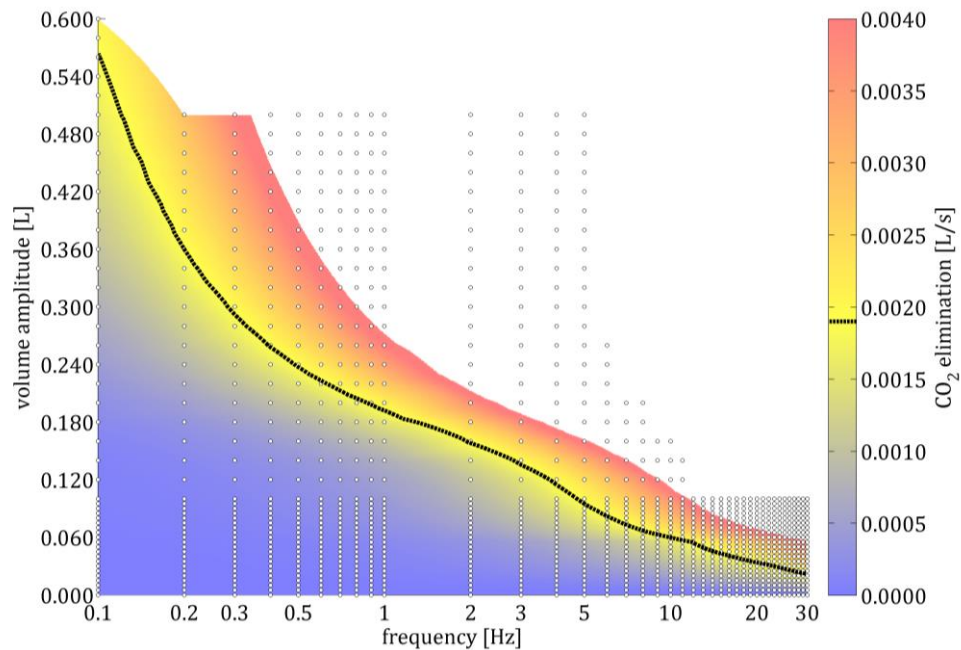


Figure 15. Interpolated contours of \dot{V}_{CO_2} over the V_T - f plane, bi-linearly interpolating between the discrete pairs of V_T and f chosen for simulations (indicated by white circles). The black line indicates the prediction of required \dot{V}_{CO_2} for eucapnia.

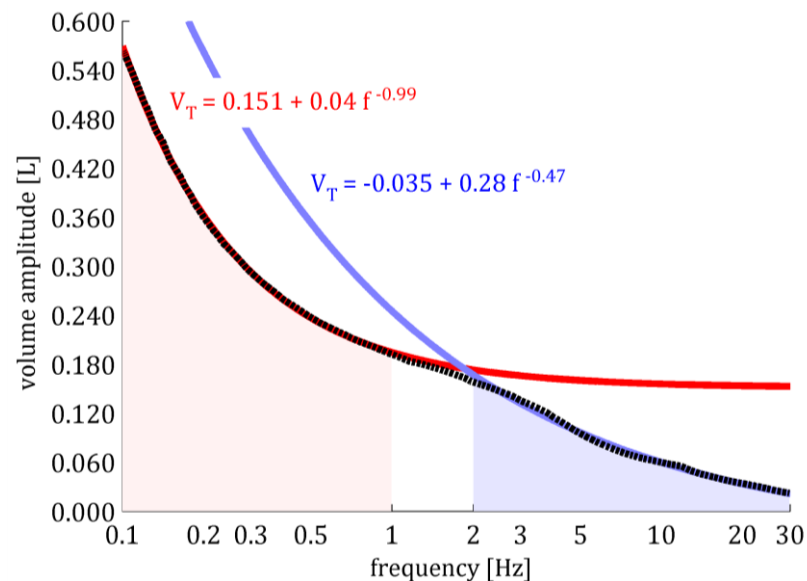


Figure 16. Power-law regressions to eucapnic tidal volume requirements over localized frequency ranges. The black line represents the interpolated contour of eucapnic ventilation parameters. The red line is regressed over $0.1 \text{ Hz} < f < 1 \text{ Hz}$, and the blue line over $2 \text{ Hz} < f < 30 \text{ Hz}$. These frequency ranges are indicated by light shading.

Figure 15 shows a contour of the required V_T for eucapnic ventilation as a function of frequency, $V_T^{\text{euc}}(f)$. Figure 16 shows power-law regressions to $V_T^{\text{euc}}(f)$ over localized frequency domains: $0.1 \text{ Hz} < f < 1 \text{ Hz}$ and $2 \text{ Hz} < f < 30 \text{ Hz}$. The regression curves are extended beyond the fit domains to demonstrate the relative reductions in required volume amplitudes that occur inside each range (compared to the extrapolated fit of the other range). In order to emphasize the deviation of \dot{V}_{CO_2} at high frequencies from the low-frequency paradigm of ventilation and gas exchange (given in Equation 1), a power-law regression was performed on the interpolated $V_T^{\text{euc}}(f)$ for $f < 1 \text{ Hz}$, using a least-squares approach to minimize the sum of squared residuals *via* numerical optimization.

$$V_T^{\text{euc}}(f) = \beta_0 + \beta_1 f^{\beta_2} \quad \text{Equation 57}$$

A regression of the form in Equation 57 produced parameter estimates $\hat{\beta}_0 = 0.151$, $\hat{\beta}_1 = 0.043$, and $\hat{\beta}_2 = -0.988$, with mean squared residual $1.5 \times 10^{-6} \text{ L}^2$. Comparing these parameter estimates to expected values requires rearranging Equation 1 to obtain:

$$V_T^{\text{euc}}(f) - V_D \propto \frac{\dot{V}_{\text{CO}_2}^{\text{euc}}}{f} \quad \text{Equation 58}$$

with the constant of proportionality taken from the p_{CO_2} equation (Equation 55), such that:

$$V_T^{\text{euc}}(f) - V_D = \frac{863 \dot{V}_{\text{CO}_2}^{\text{euc}}}{\text{PaCO}_2 f} \quad \text{Equation 59}$$

which then rearranges into the form of Equation 57:

$$V_T^{\text{euc}}(f) = V_D + \left(\frac{863 \dot{V}_{\text{CO}_2}^{\text{euc}}}{\text{PaCO}_2} \right) f^{-1} \quad \text{Equation 60}$$

The expected parameter values and the regression estimates are summarized in Table 1. The regression analysis is in close agreement with theoretical expectations pertaining to the relationship of \dot{V}_{CO_2} with respect to V_T and f at low frequencies, i.e., during conventional mechanical ventilation and spontaneous breathing.

Table 1. Regression parameters of Equation 57, expected and estimated values for low-frequencies ($f < 1$ Hz).

Parameter	Expected value	Regression estimate	Deviation from expected value [%]
β_0	0.169	0.151	10.7
β_1	0.046	0.045	2.2
β_2	-1	-0.99	1.1

For high frequencies (i.e. $2 \text{ Hz} < f < 30 \text{ Hz}$), it was found that another power-law relationship appropriately described the relationship: in this case with parameter estimate $\hat{\beta}_2 = -0.4705$ and mean squared residual $7.7 \times 10^{-6} \text{ L}^2$. This parameter estimate confirms the expectation in Equation 2 during HFOV, that the exponent of V_T is larger than the exponent of f . In this case $\dot{V}_{\text{CO}_2} \propto f^a V_T^b$ with $a = 0.47b$, or $b = 2.13a$. However, this power-law regression over-estimated the values of $V_T^{\text{euc}}(f)$ for $f > 12 \text{ Hz}$.

Finally, Figure 17 shows a comparison between the interpolated eucapnic simulation results and experimental data (97). The present simulation results, when converted to the dimensionless forms Q and \mathcal{F} from Equation 3 and Equation 4 in Section 1.1.2, demonstrate close qualitative agreement with the experimental data of Venegas *et al.*, with the largest discrepancy at the highest frequencies ($\mathcal{F} > 50 \Rightarrow f > 10.7$ Hz).

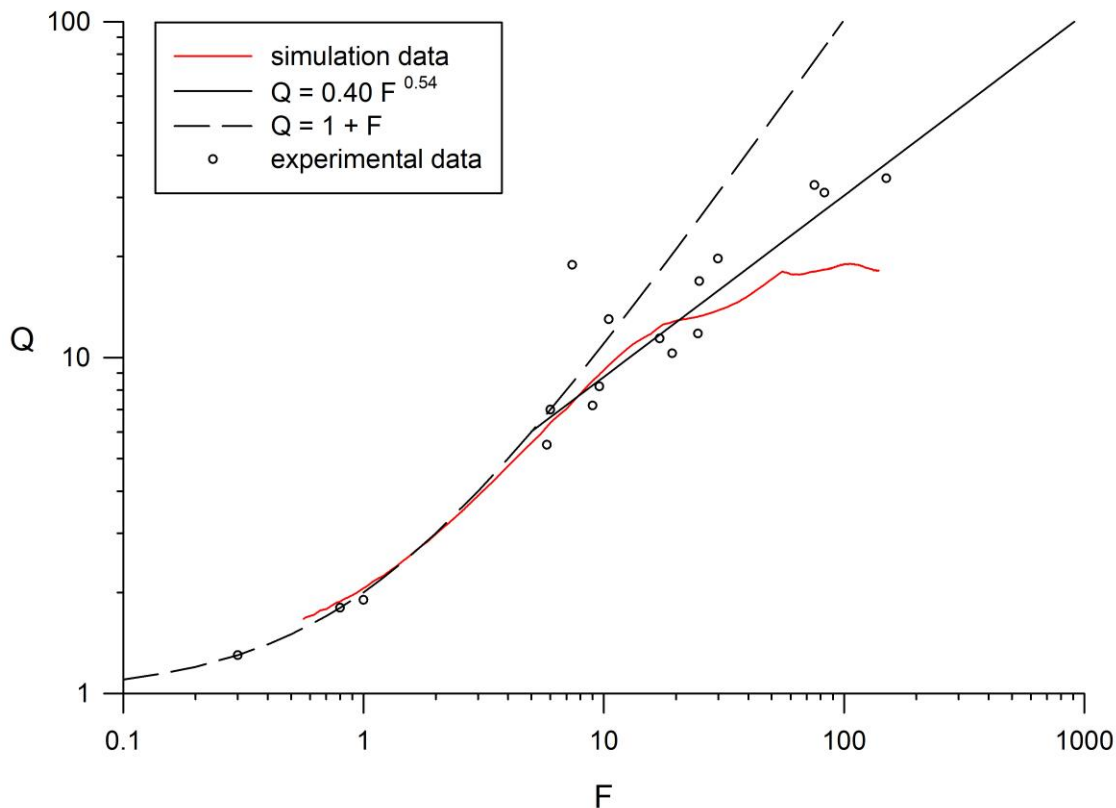


Figure 17. Comparison between the simulation data from this model and the experimental data collected and regressed by Venegas *et al.* (97). The axes are dimensionless variables of frequency (\mathcal{F}) and flow (Q). The black lines correspond to theoretical prediction of low-frequency gas exchange (dashed) and regression to experimental HFOV data (solid). The red line represents the simulation results interpolated at eucapnic conditions.

3.2. IMPACT OF MECHANICAL HETEROGENEITY

The second goal, stated in Specific Aim 2, was to investigate how imposing a heterogeneous distribution of tissue elastance H in the model alters the distribution of ventilation and gas transport. Figure 18 and Figure 19 show histograms of the ventilation distribution across a range of frequencies between 0.1 Hz and 100 Hz, color-coded according to the number of acini in the model. For both healthy and injured conditions, when $f < f_{\text{res}}$ ventilation distribution is frequency-independent. When $f > f_{\text{res}}$ ventilation distribution is both frequency-dependent and heterogeneous, even in the mechanically homogeneous healthy case. The low-frequency ventilation distribution is much more homogeneous for the healthy case compared to the injured case, as expected. However the effect of high frequency on ventilation heterogeneity is comparable between the two conditions, in both cases increasing heterogeneity with increasing $f > f_{\text{res}}$.

Multi-modal patterns are visible in the histogram data of Figure 18 and Figure 19, reflecting large groups of acini with similar frequency-dependent behavior. To assess the anatomic nature of this grouping, we visualized the groups by coloring individual acini according to the frequency at which each experiences either a minimum (f_{min}) or maximum (f_{max}) normalized flow magnitude.

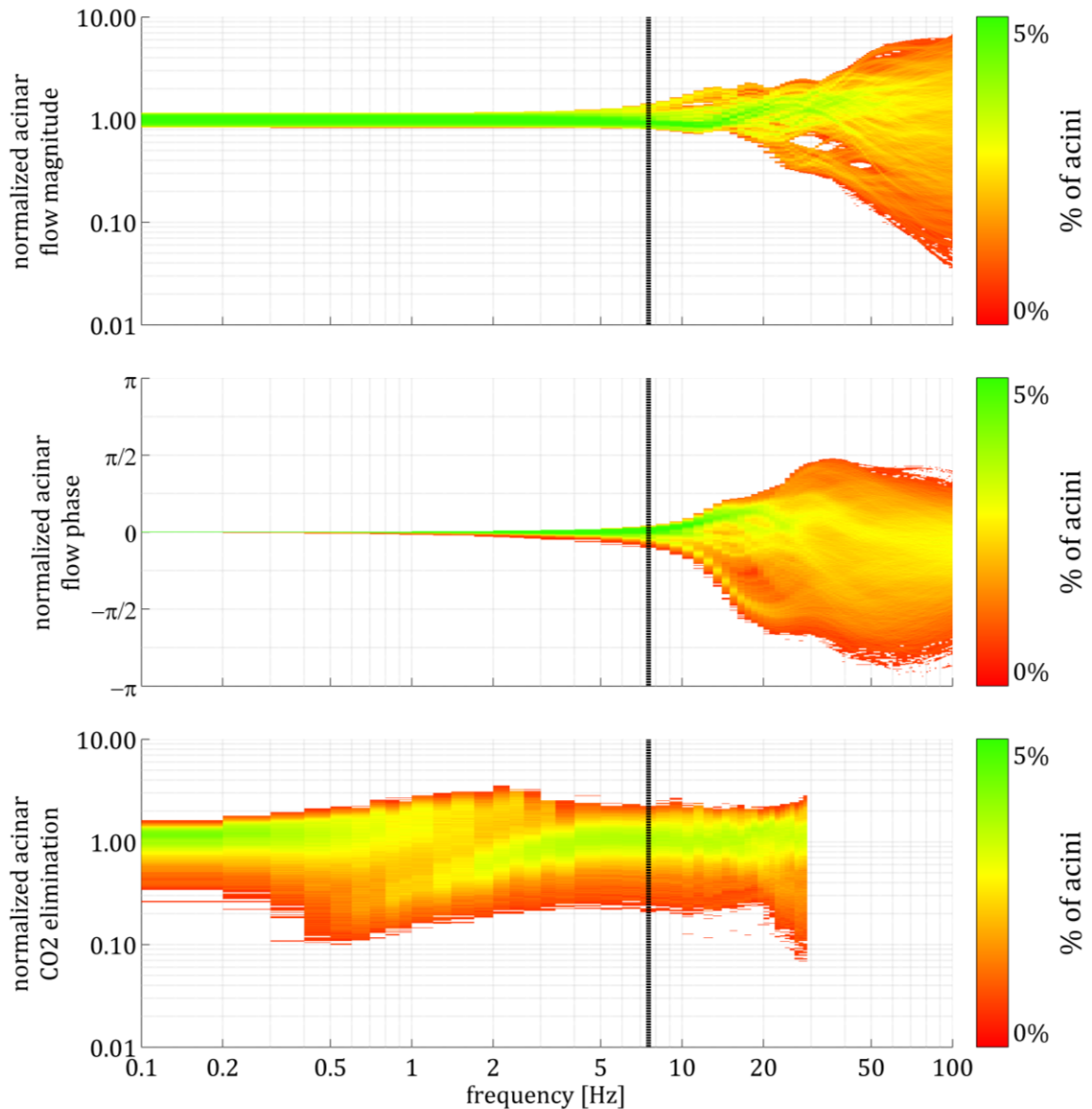


Figure 18. Acinar distribution histograms at each simulated frequency for healthy conditions. Flow magnitude (top) is normalized to a uniform distribution (i.e. unity corresponds to acinar magnitude equal to tracheal magnitude divided by the total number of acini). Flow phase (middle) is normalized to the phase of the input flow at the trachea (i.e. zero corresponds to acinar flow in phase with tracheal flow). CO_2 elimination (bottom) is normalized to a uniform distribution (i.e. unity corresponds to acinar \dot{V}_{CO_2} equal to $\dot{V}_{\text{CO}_2}^{\text{euc}}$ divided by the total number of acini). Vertical black line indicates resonant frequency (f_{res} : elastic and inertial components of impedance equal and opposite).

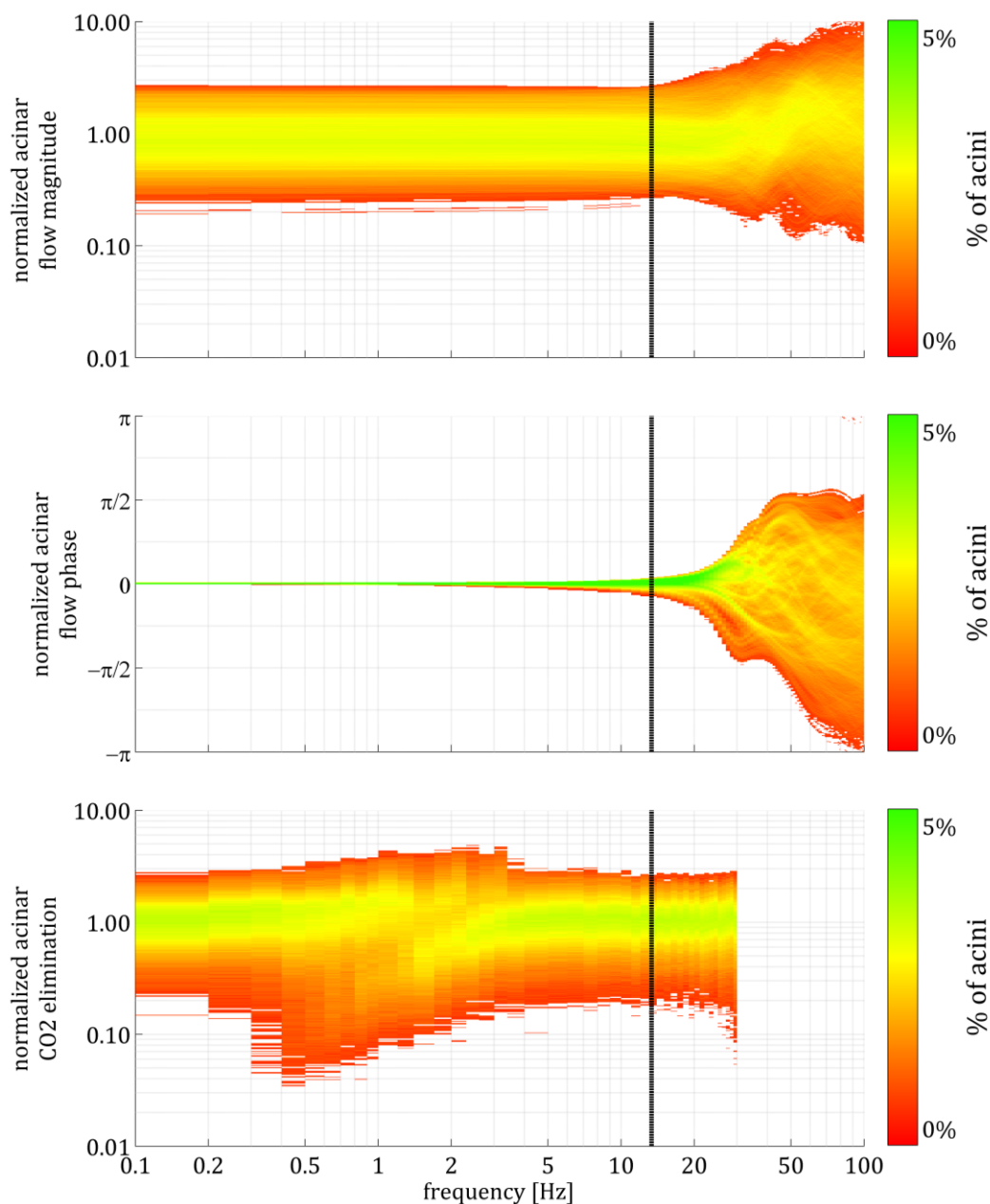


Figure 19. Acinar distribution histograms at each simulated frequency for injured conditions. Flow magnitude (top) is normalized to a uniform distribution (i.e. unity corresponds to acinar magnitude equal to tracheal magnitude divided by the total number of acini). Flow phase (middle) is normalized to the phase of the input flow at the trachea (i.e. zero corresponds to acinar flow in phase with tracheal flow). CO_2 elimination (bottom) is normalized to a uniform distribution (i.e. unity corresponds to acinar \dot{V}_{CO_2} equal to $\dot{V}_{\text{CO}_2}^{\text{euc}}$ divided by the total number of acini). Vertical black line indicates resonant frequency (f_{res} : elastic and inertial components of impedance equal and opposite).

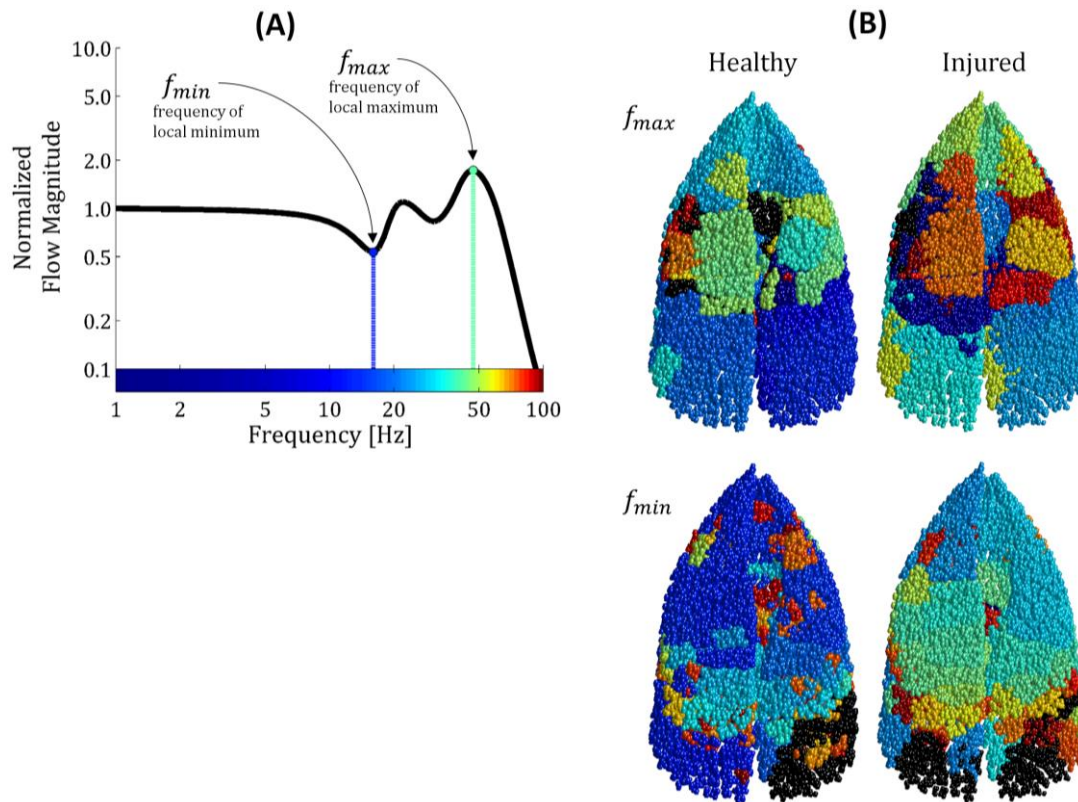


Figure 20. (A) Frequencies of maximum and minimum normalized flow magnitude, shown for clarity in the context of a single acinus. (B) Frequencies of maximum (top) and minimum (bottom) normalized flow magnitude, represented spatially for every acinus, using consistent coloring according to the scale provided in (A). Acini which do not exhibit a local minimum or maximum within the range of frequencies simulated are shown in black. Results shown for healthy (left) and injured (right) conditions.

Figure 20 (A) illustrates the concept of f_{min} and f_{max} , while Figure 20 (B) shows the spatial anatomic distributions of f_{min} and f_{max} . Spatially-organized clusters of acini with the same f_{min} or f_{max} values are immediately apparent, implying that over-ventilation and under-ventilation manifest within large regions of the lung in a frequency-dependent manner. Note that sharing the same value of f_{max} does not imply also sharing the same value of f_{min} , suggesting that subtle differences between mechanical properties of neighboring acini produce noticeable differences in frequency-dependence of ventilation distribution. Also

healthy and injured conditions exhibit similar clustering, suggesting that the frequency-dependent behavior of ventilation distribution is largely determined by airway properties affecting inertance (i.e. airway size, path-length between airway opening and acinus, airway network topology) rather than by tissue properties in this particular model of injury.

3.3. COMPARISON OF SINGLE AND MULTIPLE FREQUENCY OSCILLATION

In order to identify plausible candidate frequency pairs for multiple-frequency simulations, each combination of two distinct oscillatory frequencies was considered by taking the inner product between their respective acinar ventilation distributions (VDIP: ventilation distribution inner product). Figure 21 shows the contours of VDIP for each permutation of two frequencies (f between 0.1 Hz and 50 Hz).

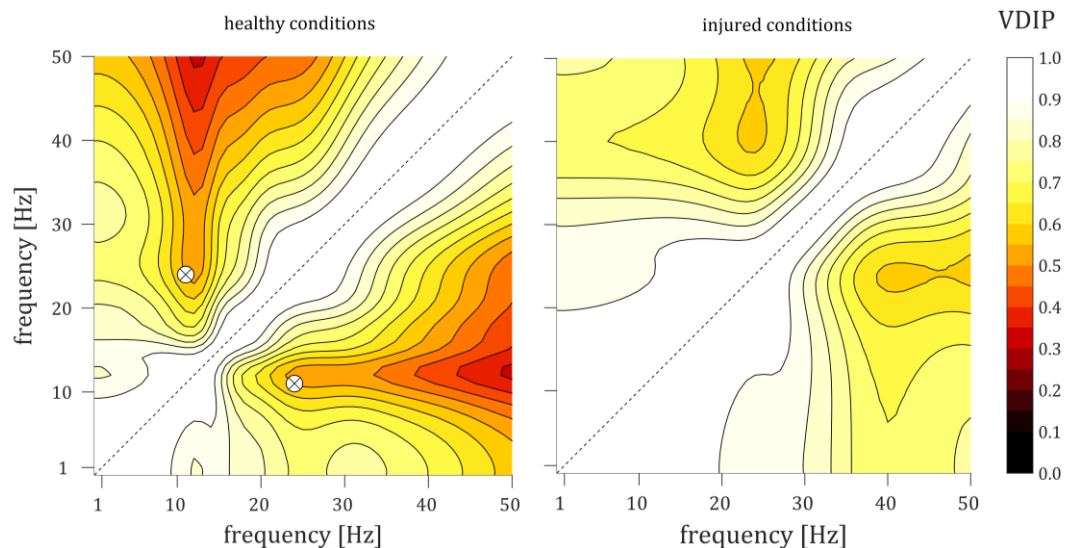


Figure 21. Ventilation distribution similarity, assessed per the contours of VDIP for each permutation of two frequencies, for healthy (left) and injured (right) conditions at mean airway pressure. Note: the values are symmetric about the line of identity $f_1 = f_2$. Frequency pairs chosen for multiple frequency oscillatory ventilation gas transport simulations indicated by crossed circles.

For reference, $VDIP = 1$ implies two identical distributions, whereas $VDIP = 0$ implies two orthogonal distributions. Identifying pairs of frequencies with the lowest degree of similarity (i.e. smallest values of $VDIP$) reveals the most complementary pairs, i.e., those pairs which are most able to compensate for each other's respective under-ventilated and over-ventilated regions. From the distributions in Figure 21, a pair of frequencies was selected for simulation of gas transport as indicated by the crossed circles, chosen to represent a low value of $VDIP$ (i.e. dissimilar ventilation distributions). Due to the limited availability of gas transport simulations between 0.1 Hz and 30 Hz, the local minimum of $VDIP$ at 11 Hz and 24 Hz for the healthy model was chosen.

Figure 22 shows representative distributions of acinar CO_2 elimination and root-mean-square volume during simulations of multi-frequency oscillatory ventilation, using the pair of frequencies indicated in Figure 21. Table 2 contains relevant simulation parameters and statistical results. The most noteworthy result of this analysis is the reduction of the 90% range of values (i.e. the range between 5% and 95% quantiles) of normalized acinar V_{RMS} attainable using a combination of two frequencies (fuchsia) compared to either frequency alone (red, blue). Specifically, the degree of heterogeneity represented by the 90% range of normalized acinar V_{RMS} is reduced by 39% compared to single frequency 11 Hz ventilation (blue), and reduced by 60% compared to single frequency 24 Hz ventilation (red). This indicates that 90% of the acini achieved a specified V_{RMS} level within a narrower range, which implies more homogeneous ventilation for a

linear combination of two frequencies.

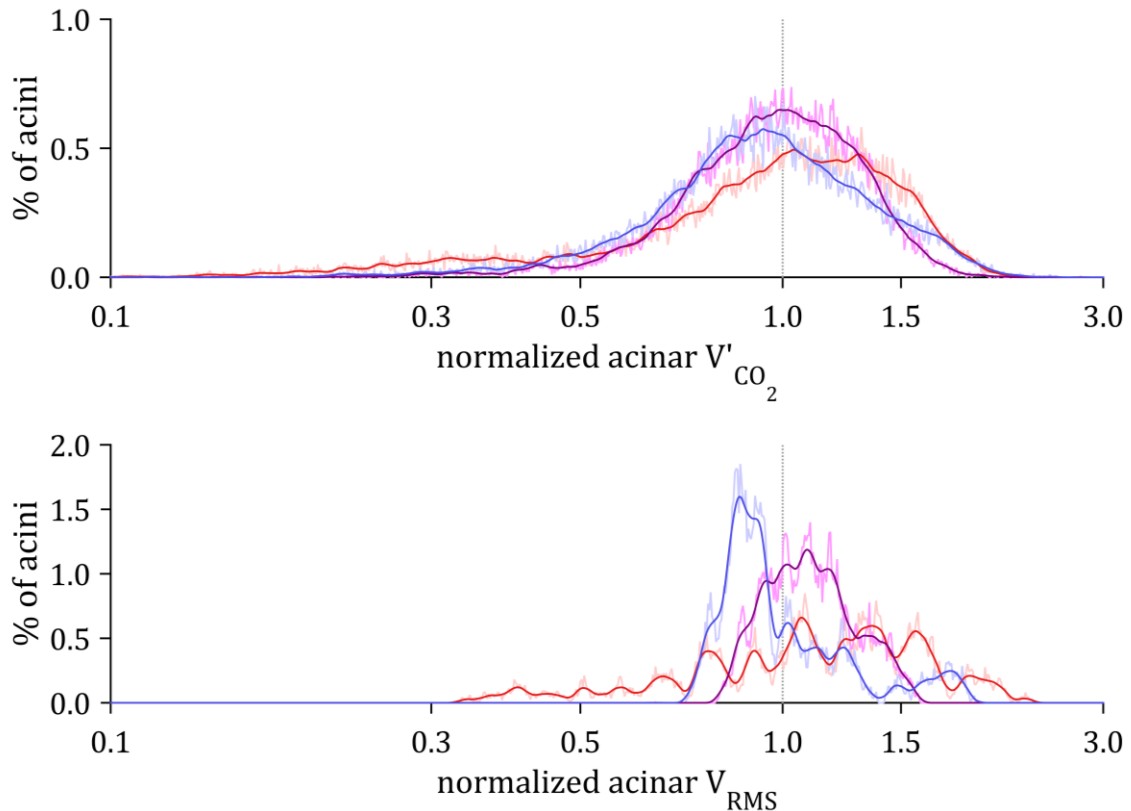


Figure 22. Histograms of acinar CO_2 elimination (top) and root-mean-square volume (bottom), normalized to the uniform distribution (i.e. unity corresponds to tracheal value divided by the total number of acini). Lightly colored lines represent raw histogram data with 1000 logarithmically spaced bins between 0.1 and 10; dark lines represent smoothed histogram data, shown for clarity. Blue: single frequency 11 Hz; red: single frequency 24 Hz; fuchsia: multi-frequency 11 Hz and 24 Hz. Histograms calculated from simulations resulting in eucapnic ventilation conditions (within 5% tolerance of $\dot{V}_{CO_2}^{euc}$). Required eucapnic tidal volume V_T for each condition and statistical results provided in Table 2.

Figure 23 shows the quantiles of normalized acinar V_{RMS} as a function of the increasing percentage of total V_{RMS} accounted for by the higher frequency. These data show that the 90% range of normalized acinar V_{RMS} is minimized when the 24 Hz oscillation accounts for approximately 35% of the total V_{RMS} . This particular combination of frequencies also minimizes the maximum value of

normalized acinar V_{RMS} . Together, these results demonstrate that for a given pair of frequencies with dissimilar ventilation distributions, a combination of the two frequencies minimizes both the heterogeneity and maximum value of normalized acinar V_{RMS} , compared to either single frequency alone.

Table 2. Simulation parameters and statistics for comparison of single- and multi-frequency ventilation. Shading indicates data represented by same colors in Figure 22.

V_T @ 11 Hz [L]	V_T @ 24 Hz [L]	total \dot{V}_{CO_2} [L/s]	deviation from $\dot{V}_{CO_2}^{euc}$ [%]	total V_{RMS} [L]	quantiles of normalized acinar V_{RMS}		
					5%	50%	95%
0.000	0.029	1.91E-03	-0.4	0.010	0.47	1.13	1.91
0.006	0.029	1.97E-03	-3.6	0.010	0.59	1.12	1.87
0.008	0.027	1.86E-03	1.9	0.010	0.65	1.12	1.85
0.013	0.025	1.82E-03	4.0	0.010	0.78	1.11	1.75
0.015	0.027	1.93E-03	-1.4	0.011	0.80	1.10	1.71
0.019	0.025	1.89E-03	0.7	0.011	0.84	1.13	1.61
0.025	0.025	1.96E-03	-3.2	0.013	0.86	1.12	1.48
0.030	0.023	1.90E-03	0.1	0.013	0.87	1.09	1.44
0.032	0.022	1.88E-03	0.8	0.014	0.87	1.08	1.45
0.038	0.019	1.84E-03	2.9	0.015	0.86	1.03	1.54
0.038	0.019	1.85E-03	2.9	0.015	0.86	1.03	1.54
0.044	0.016	1.95E-03	-2.4	0.017	0.84	0.99	1.62
0.046	0.015	1.97E-03	-3.9	0.017	0.84	0.98	1.63
0.051	0.010	1.89E-03	0.6	0.018	0.81	0.94	1.68
0.053	0.008	1.95E-03	-2.7	0.019	0.80	0.93	1.69
0.057	0.000	1.87E-03	1.8	0.020	0.78	0.92	1.71

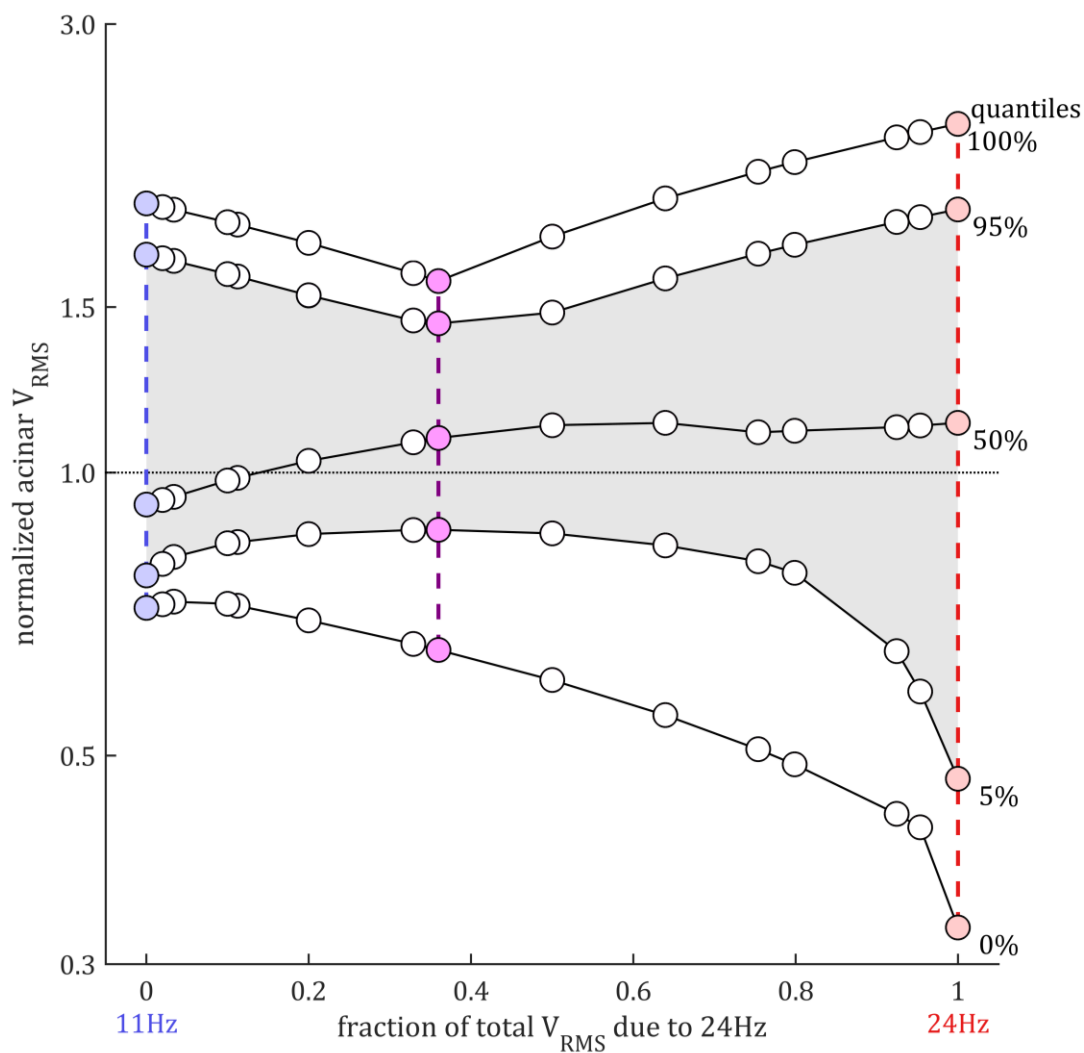


Figure 23. Quantiles of root-mean-square volume, normalized to the uniform distribution (i.e. unity corresponds to tracheal value divided by the total number of acini). Blue: single frequency 11 Hz; red: single frequency 24 Hz; fuchsia: multi-frequency 11 Hz and 24 Hz. The colored data points correspond to the histograms represented in Figure 22 and shaded cells of Table 2. The shaded gray region represents 90% of all acini. Quantiles calculated from simulations resulting in eucapnic ventilation conditions (within 5% tolerance of $\dot{V}_{\text{CO}_2}^{\text{euc}}$). Required eucapnic tidal volume V_T for each condition and statistical results provided in Table 2.

4. DISCUSSION

4.1. MODEL VALIDATION

We have developed a computational model of gas exchange during oscillatory ventilation by incorporating mechanical impedance and pertinent gas transport mechanisms over a wide range of frequencies in an anatomically-based airway network. Simulations in a healthy lung model with homogeneous mechanical properties exhibit agreement with experimental results regarding the behavior of \dot{V}_{CO_2} with respect to f , V_T , and V_D (97). The dominant mechanism of gas transport exhibits strong scaling-dependence on V_T , with transitions from molecular diffusion near zero-flow conditions to oscillatory dispersion, then turbulent dispersion, then convective mixing at bifurcations, and finally direct alveolar ventilation at the largest V_T .

The transition from oscillatory dispersion to turbulent dispersion is determined by a critical Reynolds number, which was set at $\text{Re}_{\text{crit}} = 30$ (80). Re values are proportional to the flow velocity:

$$\bar{U}_{RMS} = \frac{\pi f V_T}{2\sqrt{2}} \quad \text{Equation 61}$$

which implies dependence on both volume amplitude and frequency of oscillation. Therefore, the transition from oscillatory to turbulent dispersion occurs at different volume amplitudes for each frequency. However, oscillatory dispersion alone is not sufficient to provide eucapnic ventilation at a reasonably small V_T for any f in the simulated range between 0.1 Hz and 30 Hz. On the other hand, the transition to turbulence yields about an order-of-magnitude

increase in \dot{V}_{CO_2} compared to oscillatory dispersion. In fact, for high frequencies ($f > 10$ Hz), adequate \dot{V}_{CO_2} is achieved primarily *via* turbulent dispersion.

For frequencies between 1 Hz and 10 Hz, convective mixing at bifurcations contributes the next dramatic increase in gas transport, almost doubling \dot{V}_{CO_2} compared to gas transport *via* only turbulent and oscillatory dispersion. Because the increase in \dot{V}_{CO_2} with convective mixing at bifurcations is only approximately two-fold, it may not be fair to refer to this as a “dominant mechanism”. Instead we should consider the dispersion effects and the bifurcations effect comparable at this range of V_T and f . Unlike turbulence, the transition to convective mixing at bifurcations occurs at constant V_T across all frequencies (between 50 mL and 60 mL). The trachea of this airway network has a luminal volume of 56.3 mL, which is by far the largest volume of any airway in the model: the next largest is 6.5 mL, followed by 2.2 mL. Therefore, we may safely assume that convective mixing at bifurcations has the greatest effect on gas transport for V_T larger than the volume of the trachea.

The final transition in dominant gas transport mechanisms is attributable to the increasing prevalence of direct alveolar ventilation. Occurring at only the largest V_T , this mechanism requires a front of fresh gas to move directly between the airway opening and the acinar compartments, producing substantial gas transport *via* advection. This transition occurs more slowly than the others, due to differences in the ventilation distribution as well as the distribution of path lengths. Yet despite gaining influence only slowly, the impact of direct alveolar

ventilation on gas transport is also much larger than that of any other mechanism for CO₂ elimination by almost an order-of-magnitude.

The last two transitions seem to have constant V_T thresholds, whereas the diffusion and dispersion transitions are f -dependent as well as V_T -dependent. This can be explained by the physical dependence of direct alveolar ventilation and convective mixing at bifurcations on the size and arrangement of dead space in the conducting airways, whereas dispersion depends more strongly on the magnitude, frequency, and cross-sectional profile of the flow waveform.

There is currently no precedent in the literature for experimental or theoretical benchmarks of gas exchange during ventilation with multiple superimposed frequencies of oscillation. Therefore comparisons with existing experimental data are only possible for traditional HFOV and CMV.

4.2. IMPACT OF MECHANICAL HETEROGENEITY

The ventilation distribution is frequency-independent below f_{res} , yet becomes both frequency-dependent *and* spatially heterogeneous above f_{res} , even in the case of mechanically homogeneous (healthy) lungs. This change in behavior is due to transitions from elastically-dominated flow to inertially-dominated flow. The transition frequency varies regionally depending on the arrangement of mechanical impedances in the airway network. For instance, inertial properties are strongly determined by the structural topology of conducting airways, which explains why the patterns of f_{min} and f_{max} in Figure 20 are clustered according to spatial arrangement. This further explains why the clustering patterns do not

change between the healthy and injured conditions, because our simulated injury was implemented only *via* modified tissue elastances, without adjusting the mechanical properties or sizes of the conducting airways. Ventilation distribution is determined by the distribution of mechanical impedances, such that the flow to a particular acinus depends on the impedance of the path leading to that acinus relative to the impedance all other paths in the network. Therefore, minor differences in regional mechanical properties can lead to increased or decreased flow to local acini, relative to the rest of the lung at one or more particular frequencies. This analysis of f_{min} and f_{max} demonstrates that this behavior is spatially clustered, suggesting that the effect depends primarily on inertial properties of airways leading to a cluster of acini, rather than the elastic properties of those acini.

Despite producing no significant decrease in ventilation heterogeneity, higher frequencies reduced gas transport heterogeneity. In fact, ventilation heterogeneity increased. This can be attributed to the pervasive effects of mixing and dispersion, compared to the isolated impact of direct alveolar ventilation. That is, mixing and dispersion seem to be less affected by disparities in ventilation when compared to bulk advection. Thus even though the ventilation heterogeneity does not decrease in terms of flow distribution, the \dot{V}/\dot{Q} matching *appears* to improve due to the homogenization of gas transport throughout the lungs. This does not imply a reduced risk of VILI due to cyclic overdistention in localized lung regions. These simulations predict that ventilation heterogeneity

always increases for $f > f_{\text{res}}$ during traditional HFOV, either under healthy conditions or injury. As a result, despite requiring smaller volume amplitudes to achieve eucapnia, HFOV also causes much larger cyclic volume stretching in some lung regions compared to others. Thus we conclude that improvements in gas transport homogeneity during HFOV come at the cost of increased risk of parenchymal overdistention. Such behavior offers a plausible explanation for the outcomes of clinical trials that demonstrate improvements in gas exchange despite no improvement in mortality (22, 27, 47).

4.3. COMPARISON OF SINGLE AND MULTIPLE FREQUENCY OSCILLATION

The results presented in Section 3.3 demonstrate that for a given pair of frequencies with dissimilar ventilation distributions, a combination of the two minimizes both the maximum value of normalized acinar V_{RMS} , and the range between 5% and 95% quantiles, compared to either single frequency alone. We conclude that for certain pairs of frequencies with complementary ventilation distributions, it is possible to achieve eucapnia with less ventilation heterogeneity, by oscillating with a linear combination of both frequencies simultaneously. This finding has utility for the assessment and treatment of patients with heterogeneous lung injury, because simultaneous multiple frequencies can potentially minimize the extremes of cyclic acinar distension (see Figure 23), thereby reducing the risk of VILI in those lung regions. The choice of frequencies in this study was limited to one pair, located near a local minimum of the VDIP distribution, with relatively more dissimilar ventilation distributions

compared to other nearby pairs of frequencies. The pair that was chosen was based on the prediction that dissimilar ventilation distributions can be superimposed to yield more uniform flow delivery, thereby providing the same gas exchange for less injurious ventilation. However, the limited selection of only one pair of frequencies in this thesis does not consider the effects of each individual frequency on the gas transport mechanisms. Instead these simulations consider only the effects of frequency on the distribution of flow.

This analysis of multiple frequencies for ventilation examines only one particular pair of frequencies, to demonstrate the plausibility of using a multi-frequency approach compared to traditional HFOV as well as to estimate the magnitude of improvement. The results of these simulations warrant further investigation, involving optimization of the spectral content in oscillatory waveforms. Such an optimization procedure may involve an evaluation of the ventilation distribution similarity, similar to that presented in Figure 21. Clinical applications would require real-time assessment of mechanical heterogeneity. Non-invasive estimation of mechanical heterogeneity is possible using forced oscillations to estimate mechanical impedance, followed by inverse modeling with appropriate models of heterogeneous lung function (53–55). However, before such studies in animals or patients are performed, it would be advantageous to perform additional simulations over various combinations of frequencies with both high and low values of VDIP, to fully predict and

characterize the behavior of CO₂ elimination with respect to frequency content and volume amplitude.

4.4. LIMITATIONS

Despite the attempt of this computational model to accurately simulate the complex interactions of structural geometry, topology, fluid flow, and gas transport, there are numerous assumptions and simplifications that limit the physiologic interpretation of these results.

The consistency of clustering between healthy and injured conditions draws attention to one assumption in particular: that airway mechanics are not altered by the injury. This assumption is not realistic to the pathophysiology of ARDS. However it provides a controlled comparison between the healthy and injured simulations by holding airway mechanical properties constant, thereby eliminating potential variability of dead space volume. The alterations in flow distribution and gas transport in the injured simulation are attributed only to the heterogeneous distribution of tissue elastances.

Another assumption, that mixed-venous blood has a constant partial pressure of CO₂ in all simulations, restricts the applicability of these simulations to eucapnic conditions and short time scales; in other words, all simulations are executed to calculate an instantaneous \dot{V}_{CO_2} under the premise that $p_{mv}CO_2$ is uniformly 46 mmHg throughout the lung. If the value of instantaneous \dot{V}_{CO_2} calculated in this way for any waveform is equal to the rate of CO₂ generation by metabolism, then that waveform will maintain equilibrium of blood pCO₂ values.

These results further suggest that the ventilation distribution is more sensitive to changes in mechanical heterogeneity, whereas the gas transport exhibits much less dependence. This may be due to the effectiveness of convective mixing and dispersion in the peripheral airways, even when oscillatory flow is limited. This particular model of injury does not, however, account for derecruitment or perfusion shunting, which would play a significant role in reducing overall gas exchange. In fact, no intra-tidal variations of airway and acinar mechanics are modeled.

Other limitations of this model include a lack of consideration allocated to several potentially influential gas transport mechanisms: asymmetric velocity profiles at bifurcations, differences between inspiratory and expiratory velocity profiles, cardiogenic mixing, and collateral ventilation. Despite limiting the scope of modeled mechanisms for the sake of parsimony, this work still provides comparable results to previous experimental work using HFOV.

5. CONCLUSION

5.1. SUMMARY

In this thesis, we have developed a computational model of gas transport during oscillatory ventilation, and applied this model to study the effects of frequency content on ventilatory efficiency in simulated healthy and mechanically heterogeneous conditions. Simulations of low frequency oscillatory ventilation and traditional HFOV in a healthy lung yield gas exchange predictions in agreement with experimental data, validating the model at least in the context of available benchmarks. Simulations of multi-frequency oscillatory ventilation demonstrate improvement in ventilation homogeneity for combinations of frequencies with complementary ventilation distributions, compared to either single frequency alone.

The clinical implication of this study culminates in the recommendation that use of traditional HFOV (with only a single frequency of oscillation) should be restricted to frequencies approximately equal to f_{res} . HFOV using $f < f_{res}$ or $f > f_{res}$ results in increased gas transport heterogeneity and/or ventilation distribution heterogeneity. However it may be possible to optimize the frequency content of oscillatory waveforms, by using frequencies that produce complementary ventilation distributions, such that the resultant distributions of flow and gas transport are more homogeneous compared to using any single frequency. In this case, multiple oscillatory frequencies (including those above f_{res}) could be used, exploiting mechanisms of enhanced gas transport at higher

frequencies to achieve the benefits of (1) reducing the flow cost of ventilation, and (2) improving the homogeneity of gas transport and therefore the apparent \dot{V}/\dot{Q} matching, while (3) minimizing the heterogeneity of the flow distribution and injury risk. Future work on the optimization of frequency content of oscillatory waveforms has great potential to improve the state of critical care for patients with heterogeneous lung injury.

5.2. FUTURE WORK

The fundamental purpose of this study was to investigate the impact of mechanical heterogeneity on gas exchange, i.e., to determine what effect a heterogeneous ventilation distribution has (if any) on gas transport. These results suggest that gas transport is less sensitive to mechanical heterogeneity compared to flow distribution. However, it is not clear whether a more accurate model of pathological function would serve as a better predictor of ventilatory efficiency in the presence of heterogeneous injury such as ARDS. For example, whether or not lung recruitment is influenced by the frequency content of oscillatory waveforms can be assessed in future work, by the addition of a mechanism for recruitment of acini (5). Additionally, more sophisticated models may investigate the extent to which asymmetric velocity profiles and/or cardiogenic mixing influence gas transport. Computational fluid dynamics can, for extreme computational cost, provide finely resolved solutions to mass transport within anatomic geometries and specified boundary conditions. The results of this thesis warrant further investigation of the effects of spectral

content of oscillatory waveforms, potentially in CFD and *in vivo*, as well as the design of patient-specific optimization based on estimates of mechanical impedance (53, 55).

APPENDIX

Pseudo-code for processing pipeline

	{ relevant Section }
construct airway network topology and mechanical impedance	{ 2.1.2 - 2.1.6 }
compute ventilation distribution	{ 2.1.7 - 2.1.8 }
<u>FOR</u> (each combination of f and V_T)	
compute R_T^{diff} and R_T^{mix}	{ 2.2.2 - 2.2.3 }
construct \mathbf{R}_T and compute LU factorization	{ 2.2.4 }
<u>WHILE</u> ($\Delta\mathbf{p}$ not converged)	
compute \dot{V}_{CO_2} from acini to airways	
based on $\mathbf{R}_T \dot{\mathbf{M}} = \Delta\mathbf{p}$	{ 2.2.1 }
based on $\Delta\mathbf{p}$ and direct alveolar ventilation	{ 2.2.5 }
compute \dot{V}_{CO_2} from capillaries to acini	
based on perfusion rates and arterial-venous contents	
update new $\Delta\mathbf{p}$	
based on \dot{V}_{CO_2} difference between ventilation and perfusion	
<u>END WHILE</u>	
<u>END FOR</u>	

BIBLIOGRAPHY

1. **Amini R, Kaczka DW.** Impact of ventilation frequency and parenchymal stiffness on flow and pressure distribution in a canine lung model. *Annals of Biomedical Engineering* 41: 2699–711, 2013.
2. **Aris R.** On the Dispersion of a Solute in a Fluid Flowing through a Tube. *Proceedings of the Royal Society A: Mathematical, Physical and Engineering Sciences* 235: 67–77, 1956.
3. **Armengol J, Jones RL, King EG.** Collateral ventilation during high-frequency oscillation in dogs. *Journal of Applied Physiology* 58: 173–9, 1985.
4. **Arnold JH, Hanson JH, Toro-Figuero LO, Gutiérrez J, Berens RJ, Anglin DL.** Prospective, randomized comparison of high-frequency oscillatory ventilation and conventional mechanical ventilation in pediatric respiratory failure. *Critical Care Medicine* 22: 1530–9, 1994.
5. **Bates JHT, Irvin CG.** Time dependence of recruitment and derecruitment in the lung: a theoretical model. *Journal of Applied Physiology* 93: 705–713, 2002.
6. **Berdine GG, Lehr JL, McKinley DS, Drazen JM.** Nonuniformity of canine lung washout by high-frequency ventilation. *Journal of Applied Physiology* 61: 1388–94, 1986.
7. **Bersten AD, Edibam C, Hunt T, Moran J.** Incidence and mortality of acute lung injury and the acute respiratory distress syndrome in three Australian States. *American Journal of Respiratory and Critical Care Medicine* 165: 443–8, 2002.
8. **Bohn DJ, Miyasaka K, Marchak BE, Thompson WK, Froese AB, Bryan AC.** Ventilation by high-frequency oscillation. *Journal of Applied Physiology: Respiratory, Environmental and Exercise Physiology* 48: 710–6, 1980.
9. **Bollen CW, Uiterwaal CSPM, van Vught AJ.** Systematic review of determinants of mortality in high frequency oscillatory ventilation in acute respiratory distress syndrome. *Critical Care* 10: R34, 2006.
10. **Bollen CW, van Well GTJ, Sherry T, Beale RJ, Shah S, Findlay G, Monchi M, Chiche J-D, Weiler N, Uiterwaal CSPM, van Vught AJ.**

- High frequency oscillatory ventilation compared with conventional mechanical ventilation in adult respiratory distress syndrome: a randomized controlled trial [ISRCTN24242669]. *Critical Care* 9: R430–9, 2005.
11. **Briscoe WA, Foerster RE, Comroe JH.** Alveolar ventilation at very low tidal volumes. *Journal of Applied Physiology* 7: 27–30, 1954.
 12. **Carvalho AR, Spieth PM, Pelosi P, Vidal Melo MF, Koch T, Jandre FC, Giannella-Neto A, de Abreu MG.** Ability of dynamic airway pressure curve profile and elastance for positive end-expiratory pressure titration. *Intensive Care Medicine* 34: 2291–9, 2008.
 13. **Chang HK.** Mechanisms of gas transport during ventilation by high-frequency oscillation. *Journal of Applied Physiology: Respiratory, Environmental and Exercise Physiology* 56: 553–63, 1984.
 14. **Chatwin PC.** On the longitudinal dispersion of passive contaminant in oscillatory flows in tubes. *Journal of Fluid Mechanics* 71: 513–527, 1975.
 15. **Choi J, Xia G, Tawhai MH, Hoffman EA, Lin C-L.** Numerical study of high-frequency oscillatory air flow and convective mixing in a CT-based human airway model. *Annals of Biomedical Engineering* 38: 3550–71, 2010.
 16. **Cioffi WG, Graves TA, McManus WF, Pruitt BA.** High-frequency percussive ventilation in patients with inhalation injury. *The Journal of Trauma* 29: 350–4, 1989.
 17. **Colletti AA, Amini R, Kaczka DW.** Simulating ventilation distribution in heterogenous lung injury using a binary tree data structure. *Computers in Biology and Medicine* 41: 936–45, 2011.
 18. **Colletti AA, Amini R, Kaczka DW.** Simulating Gas Exchange in the Canine Lung Using Computational Modeling. In: *American Thoracic Society International Conference*. Philadelphia, PA: 2013.
 19. **Cools F, Offringa M, Askie LM.** Elective high frequency oscillatory ventilation versus conventional ventilation for acute pulmonary dysfunction in preterm infants. *Cochrane Database of Systematic Reviews* : CD000104, 2015.
 20. **Derdak S, Mehta S, Stewart TE, Smith T, Rogers M, Buchman TG, Carlin B, Lawson S, Granton J.** High-frequency oscillatory

- ventilation for acute respiratory distress syndrome in adults: a randomized, controlled trial. *American Journal of Respiratory and Critical Care Medicine* 166: 801–8, 2002.
21. **Derdak S.** High-frequency oscillatory ventilation for acute respiratory distress syndrome in adult patients. *Critical Care Medicine* 31: S317–23, 2003.
 22. **Eastman A, Holland D, Higgins J, Smith B, Delagarza J, Olson C, Brakenridge S, Foteh K, Friese R.** High-frequency percussive ventilation improves oxygenation in trauma patients with acute respiratory distress syndrome: a retrospective review. *American Journal of Surgery* 192: 191–5, 2006.
 23. **Ebert DS, Musgrave FK, Peachey D, Perlin K, Worley S, Mark WR, Hart JC.** *Texture and Modeling: A Procedural Approach*. 3rd ed. Morgan Kaufmann Publishers, 2002.
 24. **Erickson SE, Martin GS, Davis JL, Matthay MA, Eisner MD.** Recent trends in acute lung injury mortality: 1996-2005. *Critical Care Medicine* 37: 1574–9, 2009.
 25. **Ferguson ND, Cook DJ, Guyatt GH, Mehta S, Hand L, Austin P, Zhou Q, Matte A, Walter SD, Lamontagne F, Granton JT, Arabi YM, Arroliga AC, Stewart TE, Slutsky AS, Meade MO.** High-frequency oscillation in early acute respiratory distress syndrome. *The New England Journal of Medicine* 368: 795–805, 2013.
 26. **Ferring M, Vincent JL.** Is outcome from ARDS related to the severity of respiratory failure? *The European Respiratory Journal* 10: 1297–300, 1997.
 27. **Fessler HE, Hess DR.** Respiratory controversies in the critical care setting. Does high-frequency ventilation offer benefits over conventional ventilation in adult patients with acute respiratory distress syndrome? *Respiratory Care* 52: 595–605; discussion 606–8, 2007.
 28. **Fortune JB, Wagner PD.** Effects of common dead space on inert gas exchange in mathematical models of the lung. *Journal of Applied Physiology: Respiratory, Environmental and Exercise Physiology* 47: 896–906, 1979.

29. **Fredberg JJ.** Augmented diffusion in the airways can support pulmonary gas exchange. *Journal of Applied Physiology: Respiratory, Environmental and Exercise Physiology* 49: 232–8, 1980.
30. **Freitas RK, Schröder W.** Numerical investigation of the three-dimensional flow in a human lung model. *Journal of Biomechanics* 41: 2446–57, 2008.
31. **Fukuchi Y, Roussos CS, Macklem PT, Engel LA.** Convection, diffusion and cardiogenic mixing of inspired gas in the lung; an experimental approach. *Respiration Physiology* 26: 77–90, 1976.
32. **Gajic O, Dara SI, Mendez JL, Adesanya AO, Festic E, Caples SM, Rana R, St Sauver JL, Lymp JF, Afessa B, Hubmayr RD.** Ventilator-associated lung injury in patients without acute lung injury at the onset of mechanical ventilation. *Critical Care Medicine* 32: 1817–24, 2004.
33. **Gattinoni L, Caironi P, Cressoni M, Chiumello D, Ranieri VM, Quintel M, Russo S, Patroniti N, Cornejo R, Bugeo G.** Lung recruitment in patients with the acute respiratory distress syndrome. *The New England Journal of Medicine* 354: 1775–86, 2006.
34. **Gavriely N, Butler JP.** Radial and longitudinal compartmental analysis of gas transport during high-frequency ventilation. *Journal of Applied Physiology* 60: 1134–44, 1986.
35. **Gerstmann DR, Minton SD, Stoddard RA, Meredith KS, Monaco F, Bertrand JM, Battisti O, Langhendries JP, Francois A, Clark RH.** The Provo multicenter early high-frequency oscillatory ventilation trial: improved pulmonary and clinical outcome in respiratory distress syndrome. *Pediatrics* 98: 1044–57, 1996.
36. **Glenny RW, Bauer C, Hofmanninger J, Lamm WJ, Krueger M a., Beichel RR.** Heterogeneity and matching of ventilation and perfusion within anatomical lung units in rats. *Respiratory Physiology & Neurobiology* 189: 594–606, 2013.
37. **Greenblatt EE, Butler JP, Venegas JG, Winkler T.** Pendelluft in the bronchial tree. *Journal of Applied Physiology* (August 28, 2014). doi: 10.1152/jappphysiol.00466.2014.
38. **Gu X, Wu G, Yao Y, Shi D, Song Y.** In adult acute respiratory distress syndrome patients, is high-frequency oscillatory ventilation more effective

and safer than conventional protective ventilation? a meta-analysis of randomized controlled trials. *Critical Care* 18: R111, 2014.

39. **Gupta P, Green JW, Tang X, Gall CM, Gossett JM, Rice TB, Kacmarek RM, Wetzel RC.** Comparison of high-frequency oscillatory ventilation and conventional mechanical ventilation in pediatric respiratory failure. *The Journal of the American Medical Association Pediatrics* 168: 243–9, 2014.
40. **Habib RH, Suki B, Bates JHT, Jackson AC.** Serial distribution of airway mechanical properties in dogs: effects of histamine. *Journal of Applied Physiology* 77: 554–66, 1994.
41. **Hantos Z, Daróczy B, Suki B, Nagy S, Fredberg JJ.** Input impedance and peripheral inhomogeneity of dog lungs. *Journal of Applied Physiology* 72: 168–78, 1992.
42. **Harf A, Le Gall R, Chang HK.** Mechanical ventilation with superimposed high frequency oscillation in the normal rat. *Respiration Physiology* 54: 31–40, 1983.
43. **Haskins S, Pascoe PJ, Ilkiw JE, Fudge J, Hopper K, Aldrich J.** Reference cardiopulmonary values in normal dogs. *Comparative Medicine* 55: 156–161, 2005.
44. **Hickling KG, Henderson SJ, Jackson R.** Low mortality associated with low volume pressure limited ventilation with permissive hypercapnia in severe adult respiratory distress syndrome. *Intensive Care Medicine* 16: 372–7, 1990.
45. **Hickling KG, Walsh J, Henderson S, Jackson R.** Low mortality rate in adult respiratory distress syndrome using low-volume, pressure-limited ventilation with permissive hypercapnia: a prospective study. *Critical Care Medicine* 22: 1568–78, 1994.
46. **Huang C-T, Lin H-H, Ruan S-Y, Lee M-S, Tsai Y-J, Yu C-J.** Efficacy and adverse events of high-frequency oscillatory ventilation in adult patients with acute respiratory distress syndrome: a meta-analysis. *Critical Care* 18: R102, 2014.
47. **Hurst JM, Branson RD, Davis K, Barrette RR, Adams KS.** Comparison of conventional mechanical ventilation and high-frequency ventilation. A prospective, randomized trial in patients with respiratory failure. *Annals of Surgery* 211: 486–91, 1990.

48. **Incropera FP, DeWitt DP.** *Fundamentals of Heat and Mass Transfer*. 3rd ed. John Wiley & Sons, 1990.
49. **Isabey D, Harf A, Chang HK.** Alveolar ventilation during high-frequency oscillation: core dead space concept. *Journal of Applied Physiology: Respiratory, Environmental and Exercise Physiology* 56: 700–7, 1984.
50. **Jan DL, Shapiro AH, Kamm RD.** Some features of oscillatory flow in a model bifurcation. *Journal of Applied Physiology* 67: 147–59, 1989.
51. **Kacmarek RM, Malhotra A.** High-frequency oscillatory ventilation: what large-animal studies have taught us! *Critical Care Medicine* 33: S148–S154, 2005.
52. **Kaczka DW, Brown RH, Mitzner W.** Assessment of heterogeneous airway constriction in dogs: a structure-function analysis. *Journal of Applied Physiology* 106: 520–30, 2009.
53. **Kaczka DW, Hager DN, Hawley ML, Simon BA.** Quantifying mechanical heterogeneity in canine acute lung injury: impact of mean airway pressure. *Anesthesiology* 103: 306–17, 2005.
54. **Kaczka DW, Lutchen KR, Hantos Z.** Emergent behavior of regional heterogeneity in the lung and its effects on respiratory impedance. *Journal of Applied Physiology* 110: 1473–81, 2011.
55. **Kaczka DW, Massa CB, Simon BA.** Reliability of estimating stochastic lung tissue heterogeneity from pulmonary impedance spectra: a forward-inverse modeling study. *Annals of Biomedical Engineering* 35: 1722–38, 2007.
56. **Kaczka DW, Smallwood JL.** Constant-phase descriptions of canine lung, chest wall, and total respiratory system viscoelasticity: effects of distending pressure. *Respiratory Physiology & Neurobiology* 183: 75–84, 2012.
57. **Lee WJ, Kawahashi M, Hirahara H.** Experimental analysis of pendelluft flow generated by HFOV in a human airway model. *Physiological Measurement* 27: 661–74, 2006.
58. **Lucangelo U, Fontanesi L, Antonaglia V, Pellis T, Berlot G, Liguori G, Bird FM, Gullo A.** High frequency percussive ventilation

- (HFPV). Principles and technique. *Minerva Anestesiologica* 69: 841–8, 848–51, 2003.
59. **Luo HY, Liu Y.** Modeling the bifurcating flow in a CT-scanned human lung airway. *Journal of Biomechanics* 41: 2681–8, 2008.
 60. **Lutchen KR, Gillis H.** Relationship between heterogeneous changes in airway morphometry and lung resistance and elastance. *Journal of Applied Physiology* 83: 1192–201, 1997.
 61. **Malhotra A, Drazen JM.** High-frequency oscillatory ventilation on shaky ground. *The New England Journal of Medicine* 368: 863–5, 2013.
 62. **Mauri T, Bellani G, Confalonieri A, Tagliabue P, Turella M, Coppadoro A, Citerio G, Patroniti N, Pesenti A.** Topographic distribution of tidal ventilation in acute respiratory distress syndrome: effects of positive end-expiratory pressure and pressure support. *Critical Care Medicine* 41: 1664–73, 2013.
 63. **Montgomery AB, Stager MA, Carrico CJ, Hudson LD.** Causes of mortality in patients with the adult respiratory distress syndrome. *The American Review of Respiratory Disease* 132: 485–9, 1985.
 64. **Muellenbach RM, Kredel M, Said HM, Klosterhalfen B, Zollhoefer B, Wunder C, Redel A, Schmidt M, Roewer N, Brederlau J.** High-frequency oscillatory ventilation reduces lung inflammation: A large-animal 24-h model of respiratory distress. *Intensive Care Medicine* 33: 1423–1433, 2007.
 65. **Otis AB, McKerrow CB, Bartlett RA, Mead J, McIlroy MB, Selverstone NJ, Radford EP.** Mechanical factors in distribution of pulmonary ventilation. *Journal of Applied Physiology* 8: 427–43, 1956.
 66. **Pelosi P, Brazzi L, Gattinoni L.** Prone position in acute respiratory distress syndrome. *The European Respiratory Journal* 20: 1017–28, 2002.
 67. **Permutt S, Mitzner W, Weinmann G.** Model of gas transport during high-frequency ventilation. *Journal of Applied Physiology* 58: 1956–70, 1985.
 68. **Pillow JJ.** High-frequency oscillatory ventilation: mechanisms of gas exchange and lung mechanics. *Critical Care Medicine* 33: S135–41, 2005.

69. **Plavka R, Kopecký P, Sebron V, Svihovec P, Zlatohlávková B, Janus V.** A prospective randomized comparison of conventional mechanical ventilation and very early high frequency oscillatory ventilation in extremely premature newborns with respiratory distress syndrome. *Intensive Care Medicine* 25: 68–75, 1999.
70. **Plötz FB, Slutsky AS, van Vught AJ, Heijnen CJ.** Ventilator-induced lung injury and multiple system organ failure: a critical review of facts and hypotheses. *Intensive Care Medicine* 30: 1865–72, 2004.
71. **Ranieri VM, Rubenfeld GD, Thompson BT, Ferguson ND, Caldwell E, Fan E, Camporota L, Slutsky AS.** Acute respiratory distress syndrome: the Berlin Definition. *The Journal of the American Medical Association* 307: 2526–33, 2012.
72. **Reper P, Dankaert R, van Hille F, van Laeke P, Duinslaeger L, Vanderkelen A.** The usefulness of combined high-frequency percussive ventilation during acute respiratory failure after smoke inhalation. *Burns* 24: 34–8, 1998.
73. **Reynolds O.** An Experimental Investigation of the Circumstances Which Determine Whether the Motion of Water Shall Be Direct or Sinuous, and of the Law of Resistance in Parallel Channels. *Philosophical Transactions of the Royal Society of London* 174: 935–982, 1883.
74. **Rosenberg RB, Broner CW, Peters KJ, Anglin DL.** High-frequency ventilation for acute pediatric respiratory failure. *Chest* 104: 1216–21, 1993.
75. **Rossing TH, Slutsky AS, Lehr JL, Drinker PA, Kamm RD, Drazen JM.** Tidal volume and frequency dependence of carbon dioxide elimination by high-frequency ventilation. *The New England Journal of Medicine* 305: 1375–9, 1981.
76. **Scherer PW, Haselton FR, Seybert JR.** Gas transport in branched airways during high-frequency ventilation. *Annals of Biomedical Engineering* 12: 385–405, 1984.
77. **Scherer PW, Haselton FR.** Convective exchange in oscillatory flow through bronchial-tree models. *Journal of Applied Physiology: Respiratory, Environmental and Exercise Physiology* 53: 1023–33, 1982.
78. **Scherer PW, Shendalman LH, Greene NM, Bouhuys A.** Measurement of axial diffusivities in a model of the bronchial airways. *Journal of Applied Physiology* 38: 719–723, 1975.

79. **Slutsky AS, Brown R.** Cardiogenic oscillations: a potential mechanism enhancing oxygenation during apneic respiration. *Medical Hypotheses* 8: 393–400, 1982.
80. **Slutsky AS, Drazen JM, Ingram RH, Kamm RD, Shapiro AH, Fredberg JJ, Loring SH, Lehr J.** Effective pulmonary ventilation with small-volume oscillations at high frequency. *Science* 209: 609–71, 1980.
81. **Slutsky AS, Drazen JM.** Ventilation with small tidal volumes. *The New England Journal of Medicine* 347: 630–1, 2002.
82. **Slutsky AS, Kamm RD, Rossing TH, Loring SH, Lehr J, Shapiro AH, Ingram RH, Drazen JM.** Effects of frequency, tidal volume, and lung volume on CO₂ elimination in dogs by high frequency (2-30 Hz), low tidal volume ventilation. *The Journal of Clinical Investigation* 68: 1475–84, 1981.
83. **Slutsky AS, Ranieri VM.** Ventilator-induced lung injury. *The New England Journal of Medicine* 369: 2126–36, 2013.
84. **Slutsky AS.** Gas mixing by cardiogenic oscillations: a theoretical quantitative analysis. *Journal of Applied Physiology: Respiratory, Environmental and Exercise Physiology* 51: 1287–93, 1981.
85. **Spapen H, Borremans M, Diltoer M, Gorp V Van, Nguyen DN, Honoré PM.** High-frequency percussive ventilation in severe acute respiratory distress syndrome: A single center experience. *Journal of Anaesthesiology, Clinical Pharmacology* 30: 65–70, 2014.
86. **Stapleton RD, Wang BM, Hudson LD, Rubenfeld GD, Caldwell ES, Steinberg KP.** Causes and timing of death in patients with ARDS. *Chest* 128: 525–32, 2005.
87. **Sud S, Sud M, Friedrich JO, Wunsch H, Meade MO, Ferguson ND, Adhikari NK.** High-frequency ventilation versus conventional ventilation for treatment of acute lung injury and acute respiratory distress syndrome. In: *Cochrane Database of Systematic Reviews*, edited by Sud S. Chichester, UK: John Wiley & Sons, Ltd, 2013, p. CD004085.
88. **Suki B, Barabási AL, Lutchen KR.** Lung tissue viscoelasticity: a mathematical framework and its molecular basis. *Journal of Applied Physiology* 76: 2749–59, 1994.

89. **Talmor D, Sarge T, Malhotra A, O'Donnell CR, Ritz R, Lisbon A, Novack V, Loring SH.** Mechanical ventilation guided by esophageal pressure in acute lung injury. *The New England Journal of Medicine* 359: 2095–104, 2008.
90. **Tawhai MH, Pullan AJ, Hunter PJ.** Generation of an anatomically based three-dimensional model of the conducting airways. *Annals of Biomedical Engineering* 28: 793–802, 2000.
91. **Taylor G.** Dispersion of Soluble Matter in Solvent Flowing Slowly through a Tube. *Proceedings of the Royal Society A: Mathematical, Physical and Engineering Sciences* 219: 186–203, 1953.
92. **Taylor G.** The Dispersion of Matter in Turbulent Flow through a Pipe. *Proceedings of the Royal Society A: Mathematical, Physical and Engineering Sciences* 223: 446–468, 1954.
93. **The Acute Respiratory Distress Syndrome Network.** Ventilation with lower tidal volumes as compared with traditional tidal volumes for acute lung injury and the acute respiratory distress syndrome. *The New England Journal of Medicine* 342: 1301–8, 2000.
94. **The HIFI Study Group.** High-frequency oscillatory ventilation compared with conventional mechanical ventilation in the treatment of respiratory failure in preterm infants. *The New England Journal of Medicine* 320: 88–93, 1989.
95. **Thurston GB.** Periodic Fluid Flow Through Circular Tubes. *The Journal of the Acoustical Society of America* 24: 653, 1952.
96. **Venegas JG, Fredberg JJ.** Understanding the pressure cost of ventilation: why does high-frequency ventilation work? *Critical Care Medicine* 22: S49–57, 1994.
97. **Venegas JG, Hales CA, Strieder DJ.** A general dimensionless equation of gas transport by high-frequency ventilation. *Journal of Applied Physiology* 60: 1025–30, 1986.
98. **Ventre KM, Arnold JH.** High frequency oscillatory ventilation in acute respiratory failure. *Paediatric Respiratory Reviews* 5: 323–32, 2004.
99. **Villar J, Pérez-Méndez L, Blanco J, Añón JM, Blanch L, Belda J, Santos-Bouza A, Fernández RL, Kacmarek RM.** A universal definition of ARDS: the PaO₂/FiO₂ ratio under a standard ventilatory

- setting--a prospective, multicenter validation study. *Intensive Care Medicine* 39: 583–92, 2013.
100. **Walkey AJ, Sumner R, Ho V, Alkana P.** Acute respiratory distress syndrome: epidemiology and management approaches. *Clinical Epidemiology* 4: 159–69, 2012.
 101. **Watson EJ.** Diffusion in oscillatory pipe flow. *Journal of Fluid Mechanics* 133: 233–244, 1983.
 102. **Wilson TA, Beck KC.** Contributions of ventilation and perfusion inhomogeneities to the VA/Q distribution. *Journal of Applied Physiology* 72: 2298–2304, 1992.
 103. **Womersley JR.** Method for the calculation of velocity, rate of flow and viscous drag in arteries when the pressure gradient is known. *The Journal of Physiology* 127: 553–63, 1955.
 104. **Young D, Lamb SE, Shah S, MacKenzie I, Tunnicliffe W, Lall R, Rowan K, Cuthbertson BH.** High-frequency oscillation for acute respiratory distress syndrome. *The New England Journal of Medicine* 368: 806–13, 2013.
 105. **Zambon M, Vincent J-L.** Mortality rates for patients with acute lung injury/ARDS have decreased over time. *Chest* 133: 1120–7, 2008.
 106. International consensus conferences in intensive care medicine: Ventilator-associated Lung Injury in ARDS. This official conference report was cosponsored by the American Thoracic Society, The European Society of Intensive Care Medicine, and The Société d. *American Journal of Respiratory and Critical Care Medicine* 160: 2118–24, 1999.

CURRICULUM VITAE

